What Causes Tides ?

Yongfeng Yang
Bureau of Water Resources of Shandong Province
Address: No. 127, Lishan Road, Jinan, 250014, China
Tel. and fax: +86-0531-8697-4362
E-mail: roufeng_yang@yahoo.com; roufengyang@gmail.com

Abstract Tide (the daily cycle of high and low water) has been known for thousands of years. The widely accepted theory for this movement is the attractive mechanism, that's to say, the moon's gravitational attraction yields a pair of water bulges on the earth, an earthly site will periodically pass these bugles and thus undergo alternation of high and low water as the earth spins. However, an in-depth investigation of globally tide-gauge data shows these bulges of water essentially non-existed. This suggests that tide cannot be explained by the established understanding. Here we propose, the earth's rotations about the centre of mass of the earth-moon system and around the sun create some centrifugal effects to stretch the earth's body; the spinning deformed solid earth drives its each part to regularly move up and down, giving birth to oscillation for ocean basin, generating water movement between all the parts of the basin and further the rise and fall of water levels around the globe. A test of model shows that the mean RSS (Root Sum of Squares) calculated against observation for deep ocean (34 sites) and shelf-coastal regions (41 sites) are approximately 0.32 and 0.53 cm, furthermore, the model is available for making tide prediction.

Keywords tide, wave, the earth-moon system, the centrifugal effect, deformation of solid earth, oscillating vessel, ocean basin, tide prediction

1 Introduction

1.1 A brief retrospect of tidal theories

From antiquity it has been known that coastal seas always perform daily regular water movements of rise and fall. Since these movements are closely related to the frequently coastal activities, explaining them has undoubtedly tested human wisdom. Aristotle (384-322 BC) was highly perplexed by the phenomenon and vaguely attributed it to the rocky nature of the coastline. The early Chinese considered tides as the beating of the earth's pulse and alternately, it was believed to be caused by the earth's breathing. Others thought tides were caused by the different depths of ocean water. Galileo theorized that the rotations of the earth around the sun and about its axis induced motion within the sea to generate the tides. The majority certainly linked tidal action to the influence of the moon and of the sun. Seleucus (2nd century BC) was the first to consider this connection and concluded the height of tide was correlated with the moon's position relative to the sun. However, the exact determination of how the moon

and sun caused tides was unknown. A few Arabic explanations proposed that the moon used its rays to heat and expand the water. Descartes argued that space was full of ethereal substance and the resulting stresses between the ether and the earth's surface gave birth to tides when the moon orbited the earth. In contrast, Kepler and Newton defined the action as the attraction of the moon and sun on water. Newton concluded the moon's gravitation caused a pair of water bulges on the earth. In consideration of the complexity of actual oceans and currents, Laplace developed a set of hydrodynamic equations. Together with the following endeavours (made by William Thomson, Baron Kelvin, Henri Poincaré, Arthur Thomas Doodson, etc.,), the idea of the gravitational attractions of the moon and sun on water (the attractive mechanism) was increasingly consolidated and became the cornerstone of modern tidal theories. A fuller review of tidal theory may be seen in these works (Pugh 1987; Cartwright 1999; Deacon 1971; Pugh and Woodworth 2014). Undoubtedly, the physics of tides involves in a variety of fields ranging from the orbit of celestial objects (the moon and the sun, for instance), the mixing of the oceans, solid-earth geophysics and coastal flooding (Lambeck 1988; Munk 1997; Vlasenko et al. 2005). In the past decades a rapid growth of tide models greatly facilitated spatial and ground measurements (Pekeris et al. 1969; Schwiderski 1979; Fu and Cazenave 2001; Visser et al. 2010), tidal dynamics and energy dissipation were well studied (Stammer et al. 2014), the investigation on internal tides becomes considerably active (Gargett and Hghes 1972; Phillips 1974; Shepard 1975; Garrett and Munk 1979; Gao et al. 2013; Shanmugam 2014), all these in turn help us realize a better understanding of tide. Notwithstanding, many problems remain open in the established tidal theories.

1.2 Problems of the established tidal theories

The established tidal theories may be morphologically divided into two parts: the equilibrium tide and the dynamic tide. The equilibrium tide was directly developed from the attractive mechanism, that's to say that the earth orbits about the centre of mass of the earth-moon system, this makes all particles of the earth travel around in circles which have the same radius. The force responsible for these circular or curved motions is treated as centripetal force. The centripetal force necessary to maintain each particle in this revolution is the same as for the particles at the centre. For particles nearer the moon, its gravitational attraction on them is greater than the centripetal force. Further away, the moon's gravitational attraction is weaker than the centripetal force. The difference between the centripetal force and the moon's gravitational attraction is the tide-generating force (Pugh 1987; Pugh and Woodworth 2014). The tide-generating force is further decomposed into two components respectively perpendicular and parallel to the earth's surface. The vertical can be compensated by earth's gravity, but the horizontal cannot be counteracted in the same manner and causes particles to move in the direction of the force. The net result of the tidal forces acting on a watery earth is to move water towards positions nearest to and farthest from the moon. This eventually yields two bulges of water along the earth-moon line and a depression of water in a ring around the earth halfway between the two bulges (Pugh 1987; Robert 2008; Pugh and Woodworth 2014). For an earthly site it would pass through the two bulges of water and the depression as the earth spins and hence undergoes two cycles of high and low

water per day. Similarly, another two bulges of water along the earth-sun line and another depression of water between these two bulges are also yielded due to the sun's gravitational attraction on water. When these two types of bulges and depressions are combined together, they reinforce or cancel each other to generate the two cycles of high and low water per month.

More than 300 years since the foundation of the attractive mechanism, most of people had been led by the paradigm of the two bulges of water to understand tide. However, the paradigm of the two bulges of water seems to be self-evident and has never been strictly verified. Nowadays, many large tide data collections like UHSLC (University of Hawaii Sea Level Center), PSMSL (Permanent Service for Mean Sea Level), and BODC (British Oceanographic Data Center) provide condition for us to do this work. If there were two bulges of water on the earth, there must be a thing to happen, i.e., when the earth spins around its axis, the earthly sites entering into the scope of these bulges would undergo high water. The frame of the two bulges and the moon in space can be illustrated (Fig. 1(A)). A hourly tide-gauge data of 229 globally-distributed sites are used to examine this expectation. Tide data are commonly treated as follows: water level change of a tide gauge site is the difference of the mean of all hourly water levels of this site during the month and its hourly water level. This yields a same reference frame (i.e., water level is zero) for all these data to be compared together. The result, however, extremely unexpected, disagrees to the existence of the two bulges of water. From a viewpoint of spherical geometry, we accept that these sites, if their lunar angles (that's the angle of an earthly site and the moon with respect to the earth's centre) fall into a phase of 0^{o}~45^{o} and 135^{o}~180^{o}, must have entered into the scope of the two bulges and trend to perform high water, whereas if their lunar angles fall into a phase of 45^{o}~135^{o}, they must have got out of the two bulges of water and trend to perform low water. Contrary to this, as shown in Figure 1(2), the distributions of high and low waters of all 229 tide gauge sites are highly scattered, no evidence to show a concentration of high or low water toward a special phase. The figure here exhibits only a state of 6 independent moments (0h, 4h, 8h, …, for instance) in the day of August 13, 2014. At the time, the moon is located about equator. In fact, we have checked the hourly tide data of all the sites over the whole August of 2014, all results commonly object to the existence of the two bugles of water.

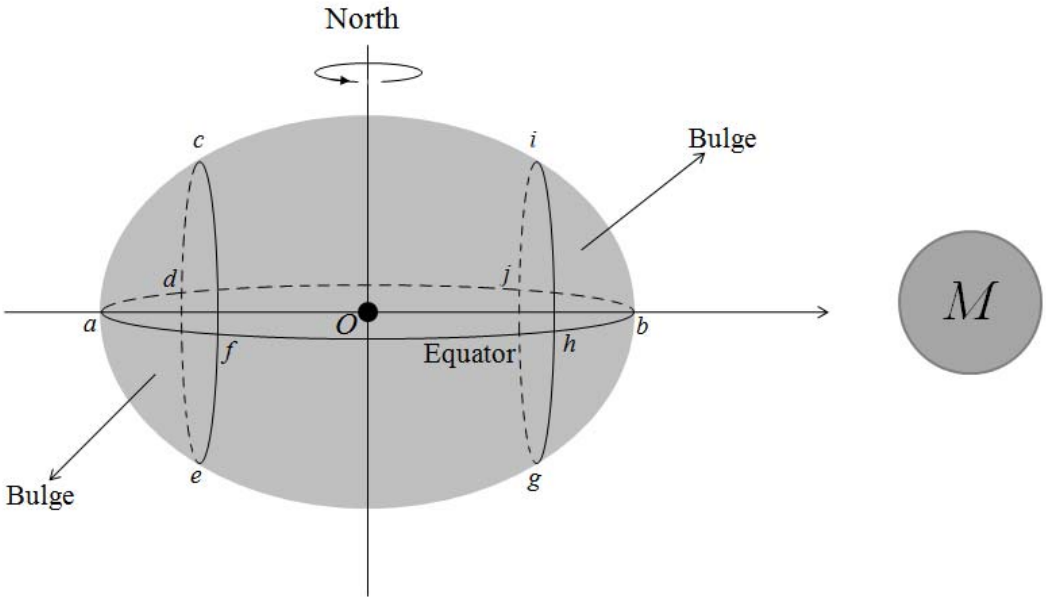
North
c
i
Bulge
d
j
a
O
b
M
f
Equator
h
Bulge
e
g

A

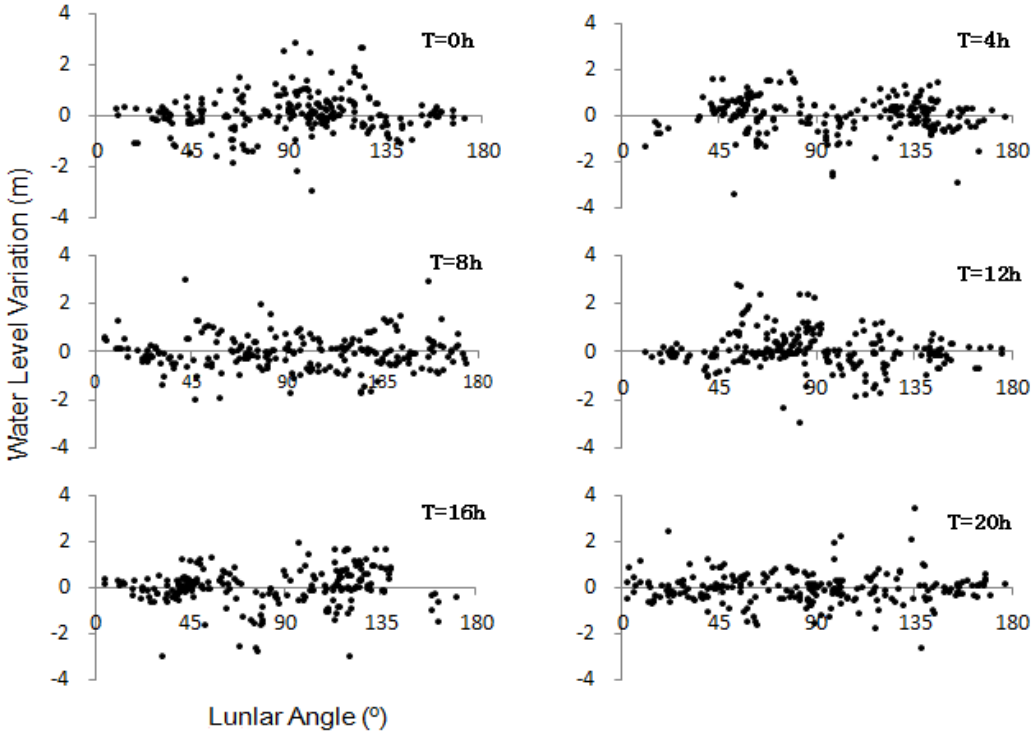
T=0h
T=4h
T=8h
T=12h
T=16h
T=20h
Water Level Variation (m)
Lunlar Angle (°)

B

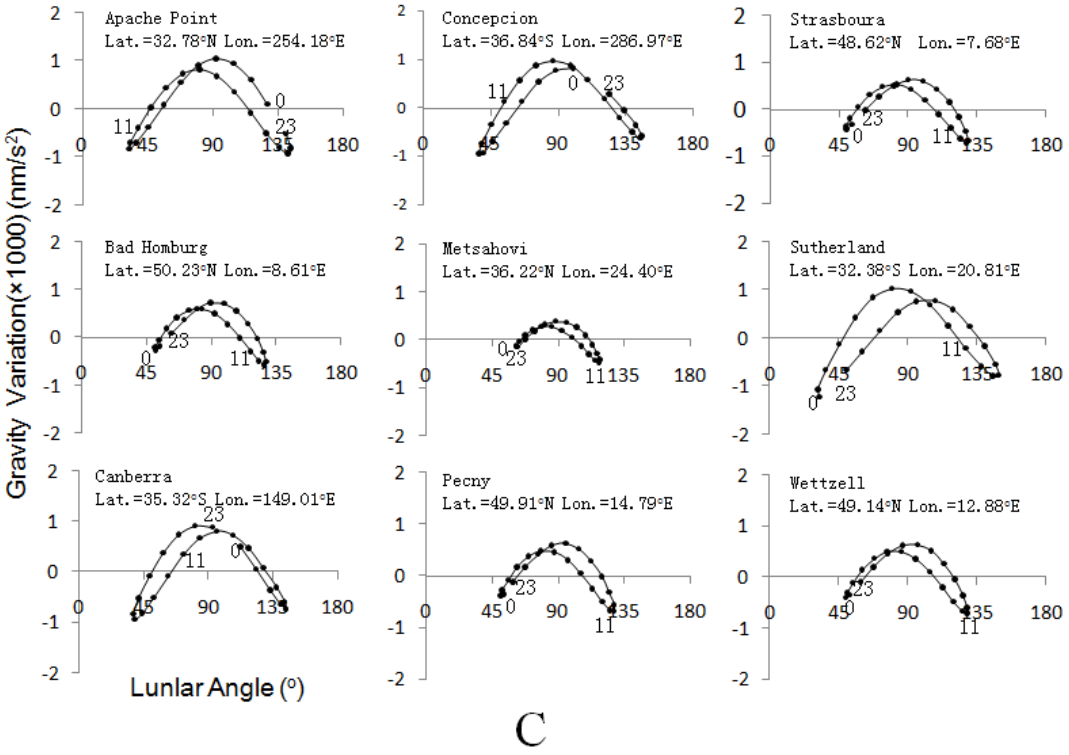

FIG. 1 Tidal bulges Versus Water Level Change. A, modelling the frame of tidal bulges and the moon in space. Area *a-cdef* and *b-ghij* denote the two bulges. *O* and *M* denote respectively the earth's centre and the moon. Note that, the deformation is highly exaggerated; **B**, water level changes of 229 tide gauge sites out to their lunar angles in the day of August 13, 2014. Tide gauge data refer to UHSLC (Caldwell et al. 2015). **C,** gravity changes of 9 gauge sites out to their lunar angles in the same day**.** In each diagram number 0, 11, and 23 respectively represent a GMT hour of August 13, 2014. Gravity data refer to IGETS (International Geodynamics and earth Tide Service) (Voigt et al. 2016).

Once the two bulges of water aren't existed, it is impossible for any earthly site to get in or out of them, and also impossible for the two types of water bugles to reinforce or cancel each other, the daily and fortnightly cycles of high and low waters immediately become unable to be explained by the established understanding. This also disables the dynamic tide, we will later discuss this point. Now, let's see what happens if we assume the two bugles of water and the depression to be existed and workable.

First of all, the structure of the two bulges of water and the depression would yield an equality of size of the two successive low waters and an inequality of size of the two successive high waters for a site. As shown in Figure 2(a), there is mechanically a ring (the depression, for instance) of lowest water around the earth halfway between the two bulges. As the earth spins around its axis, a site *P* would pass through the two bulges and the depression to undergo two low waters of same size and two high waters of different size per day. From a viewpoint of the globe, other sites like *N* and *Q* also would undergo two low waters of same size and two high waters of different size per day. On the whole, the frame of the two bulges and the depression requires high waters of all sites to be different in size and low waters to be same in size within a fixed day.

Contrary to this expectation, the low waters of all observed tides are generally different in size.

Secondly, the structure of the two bulges of water and the depression would require the two successive high (low) waters of a site to reversely develop within a lunar month, namely, for a site which is located at higher latitude, the size of its one high (low) water is increased/decreased whereas the size of its another high (low) water is decreased/increased when the two bulges transfer between north and south of equator. This point may be easily inferred from Figure 2(a). Refer to Pugh's work (1987), the tide-generating force was eventually developed into a formula below to describe the elevation of the sea surface.

$$H_m=a(M_m/M_e)[C_0(t)(3\sin^2\varphi_p/2-1/2)+C_1(t)\sin 2\varphi_p+C_2(t)\cos^2\varphi_p]$$

$$C_0(t)=(a/R_m)^3(3\sin^2 d/2-1/2)$$

$$C_1(t)=(a/R_m)^3(3\sin 2d\cos C_p/4)$$

$$C_2(t)=(a/R_m)^3(3\cos^2 d\cos 2C_p/4)$$

where H_m, a, M_m, M_e, φ_p, R_m, d, and C_p are respectively the elevation of the sea surface, the earth's radius, the moon's mass, the earth's mass, the latitude of a particle at the sea's surface, the distance of the earth and moon, the declination of the moon, and the hour angle of the particle relative to the moon.

By replacing M_m and R_m respectively with M_s (the sun's mass) and R_s (the distance of the earth and sun), the elevation of the sea surface H_s due to the effect of the sun may be got. $H_m + H_s$ therefore represent the total elevation of sea surface due to the influences of the moon and sun. Figure 2(b) exhibits several expected tides. It can be seen that, at latitude 30^oN the size of one high (low) water increases (decreases) when the size of another high (low) water decreases (increases); towards higher latitudes (60^oN and 80^oN, for instance), this asymmetry becomes considerably noticeable. Different from these, the sizes of the two successive high (low) waters of all observed tides, as shown in Figure 2(c), are alternately increased or decreased. Morphologically, there is a significant discrepancy between the expected tides and the observed tides.

Lastly, the structure of the two bulges of water and the depression would require semidiurnal tides (which have two high and two low waters of same size per day) to occur at lower latitudes, diurnal tides (which have one high water and one low water of same size per day) to occur at higher latitudes, and mixed tides (which have two high and two low waters of different size per day) to occur at middle latitudes. Contrary to these, the semidiurnal and mixed tides, as shown in Figure 2(e), are extensively distributed around the globe, only a few places (the Karumba and Mexico gulf, for instance) hold diurnal tides.

Some would like to argue that we may not employ the equilibrium tide to make comparison with observation because the responses of oceans to the tidal forces are complicated and depends on the shape of the ocean basins, the earth's rotation, and so on. A few points may overturn these arguments. On the one hand, the equilibrium tide is a net result of the attractive mechanism. If we don't employ the equilibrium tide to compare with observation, how can we conclude the gravitational attraction of the moon and sun on water to be the right cause of tide rather than other factors such as moonlight, or solar radiation, or ghost effect of a distant star to be? Actually, when the

two bugles of water are refused by observation, all addressing for the equilibrium tide becomes rather speculative and powerless. On the other hand, as shown in Figure 2(c), when the size of high or low water of a site is increased (decreased), the sizes of high or low water of other sites are at the same time increased (decreased), all these sites not only belong to different ocean but also encounter different earth's rotation in amplitude, this indicates that the evolution of high and low water is independent of these so-called external factors.

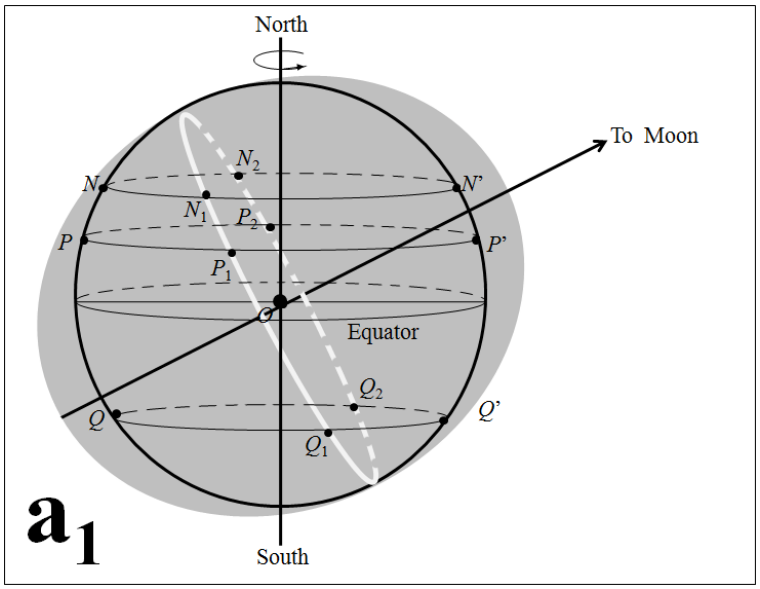

a1

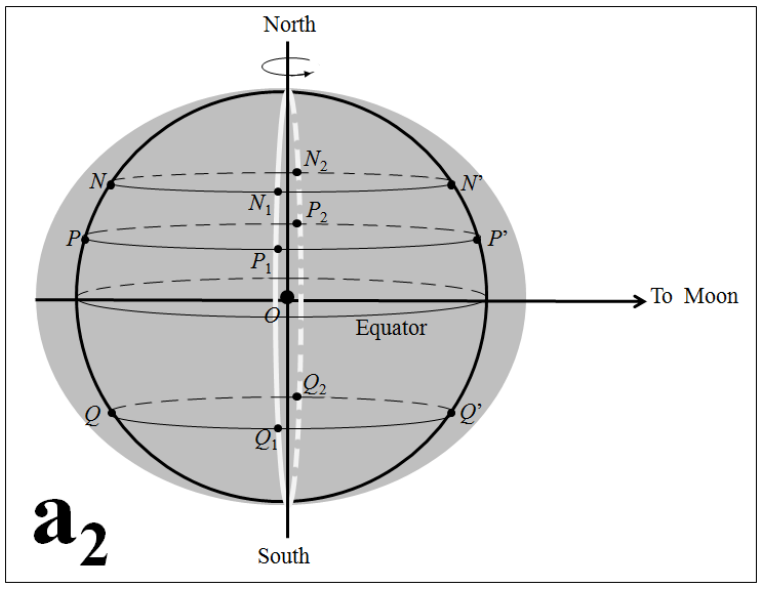

a2

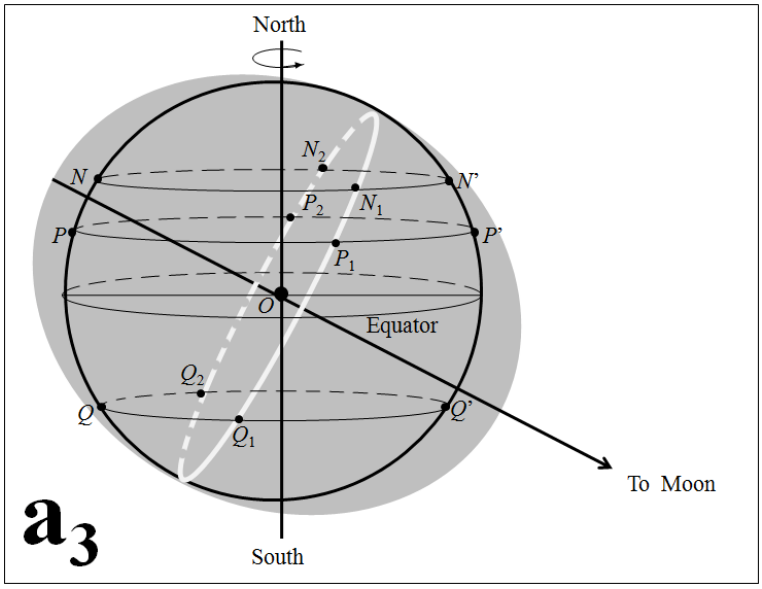
North
South
Equator
To Moon
N
N'
N_2
N_1
P
P'
P_2
P_1
O
Q
Q'
Q_2
Q_1
a3

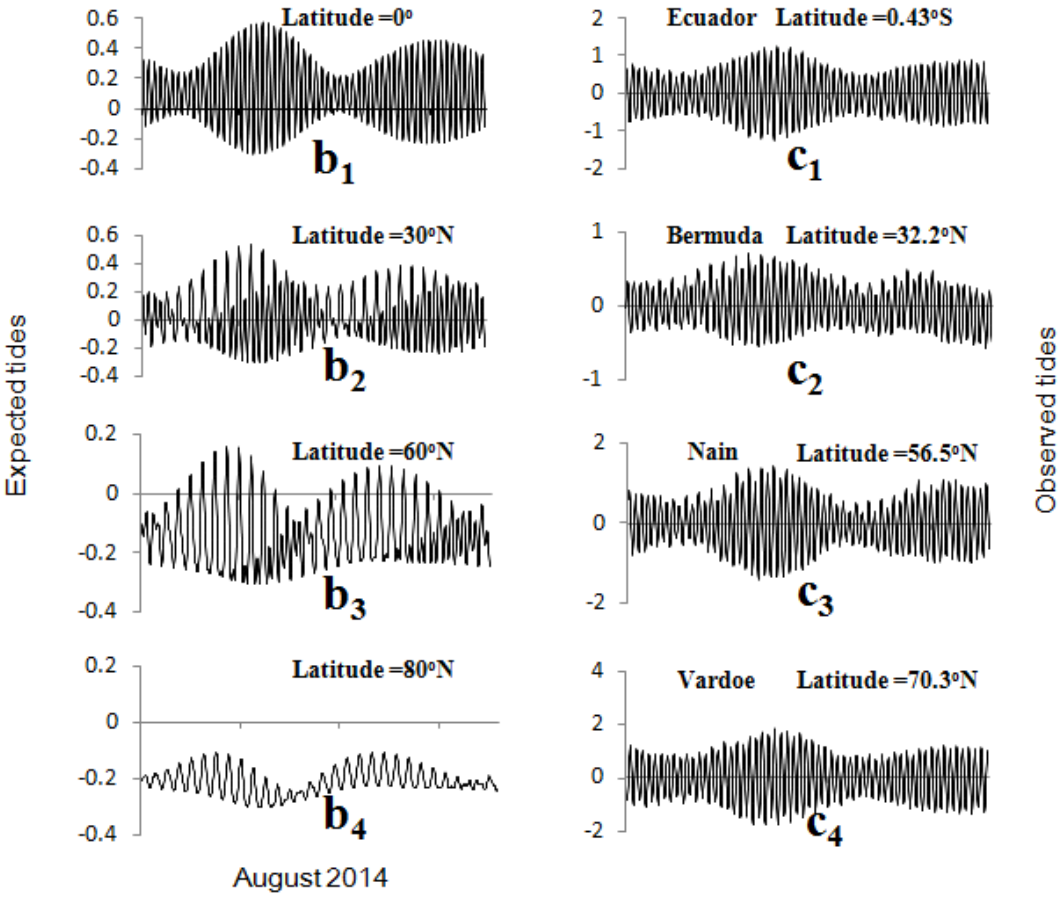
Expected tides
Observed tides
Latitude =0°
b1
Ecuador Latitude =0.43°S
c1
Latitude =30°N
b2
Bermuda Latitude =32.2°N
c2
Latitude =60°N
b3
Nain Latitude =56.5°N
c3
Latitude =80°N
b4
Vardoe Latitude =70.3°N
c4
August 2014

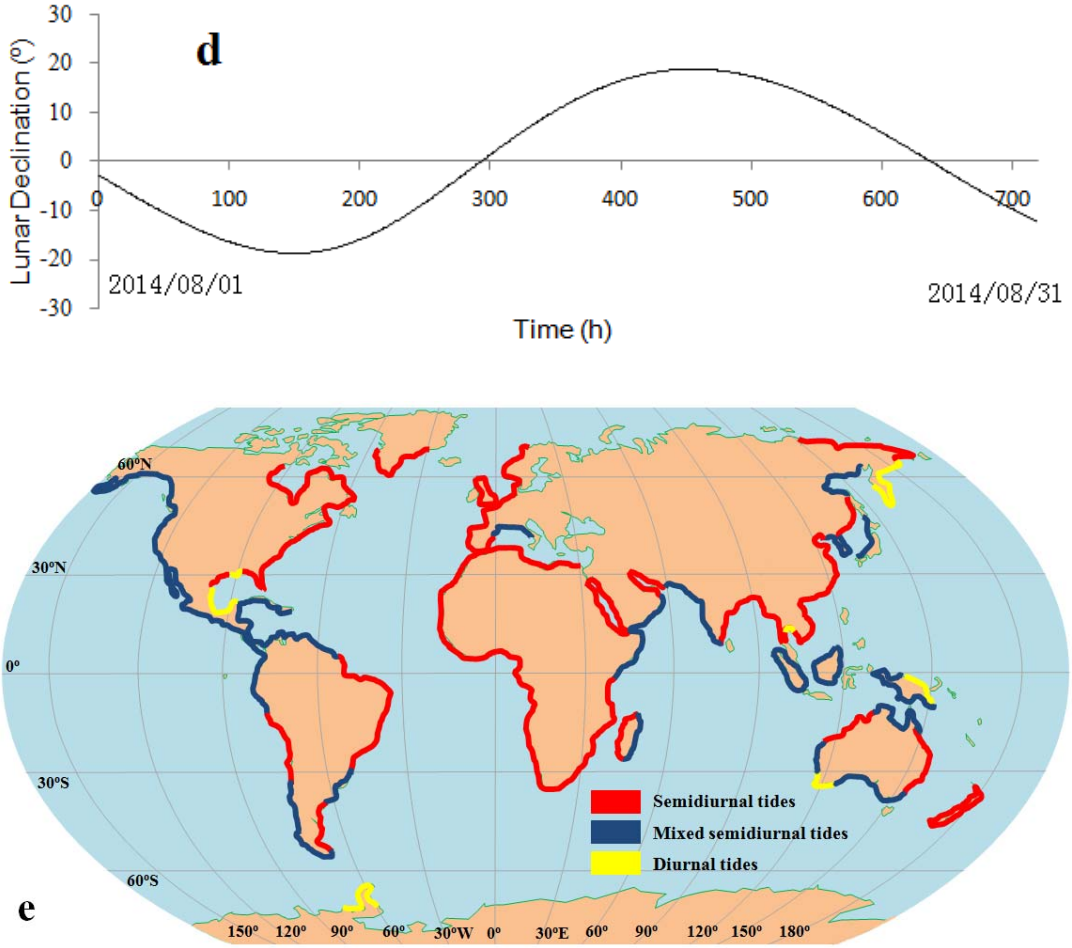

FIG. 2 Comparison of the equilibrium and observe tides. **a**, showing how the unequal high water levels and the equal low water levels are generated at various sites under the resulting two bulges. From $\mathbf{a}_1$, $\mathbf{a}_2$, to $\mathbf{a}_3$, it represents the orderly positions of the two bulges as the moon transfers from the north to the south. *O* is the earth's centre. The big circle represents an undisturbed watery planet. Note that the two bugles are seriously exaggerated; **b**, the expected tides from the tide-generating forces at different latitudes in August 2014.Vertical axis represents tidal amplitude and unit is metre; **c**, the observed tides at different latitudes during the month. Vertical axis represents tidal amplitude and unit is metre; **d**, the moon's declination during the month; **e**, tidal pattern distribution of the observed tides throughout the globe. Data supporting is from U.S. NOAA, GLOSS database - University of Hawaii Sea Level Center (Caldwell et al. 2015), and Bureau National Operations Centre (BNOC) of Australia.

The dynamic tide begins with a consideration of several factors: if there is no landmass, the two bulges of water would continuously track from east to west with the earth's daily rotation. The presence of landmasses breaks off this progression. Most of the continents are oriented in the north-south direction, the travelling tidal wave would encounter continents, generating a reflection of tidal wave. From deep oceans to shelf seas, water becomes shallower, the slope of sea floor also greatly disperses and refracts tidal waves. Moreover, the Coriolis force deflects tidal waves to right in the direction of motion in the northern hemisphere and to left in the southern hemisphere. Within the constraint of the influences of these factors, the dynamic tide was developed. An earlier

treatment of this matter was made by Laplace who expanded the equilibrium tide into a set of hydrodynamic equations of continuity and momentum. He assumed spherical earth to be with a geocentric gravitational field, a rigid ocean bottom, and a shallow ocean, which allowed Coriolis accelerations to be neglected (Pugh 1987; Pugh and Woodworth 2014). These equations are latterly followed by a series of ideas such as progressive and standing wave, resonance, Kelvin wave, and amphidromic system. As we know, wave has crest (high) and trough (low), this resembles the shape of tide (high and low water), treating tide as wave is therefore acceptable. Wave can propagate, reflect, and refract. If the frequencies of two waves near to each other, a resonance between them may amplify amplitude. A long progressive wave can be constrained by a combination of Coriolis force and shore to form a Kelvin wave. Kelvin wave often moves cyclonically around a basin. Especially, at the boundary of a basin two Kelvin waves travelling in opposite directions can be seen forming an amphidromic system. Based on these theoretical ideas, a general understanding for tides is achieved: ocean tides are generated directly by the external gravitational forces, the continental shelf tides were generated by co-oscillation with oceanic tides (Pugh 1987; Pugh and Woodworth 2014).

Careful readers would find that, the equilibrium tide tells why it occurs the alternation of high and low water on the earth whereas the dynamic tide tells how the high and low water moves around the earth. But essentially, the equilibrium tide is the source of the dynamic tide. Once the two bulges of water and the depression, which represent the equilibrium tide, are refused, the dynamic tide becomes groundless. Actually, the dynamic tide hasn't yet resolved the problems of the equilibrium tide, except for a introduction of resonance mechanism which attempts to deal with the problem of tidal range difference. The tidal range expected from the equilibrium tide is about 0.5 m at equator, but in the main oceans the observed tides have a range of about 0.0~1.0 m, in the continental shelf seas a much larger range of tides are found, at some places (the Bay of Fundy and the Argentine shelf, for instance) the tidal ranges even may reach 10.0 m (Pugh 1987; Pugh and Woodworth 2014). The resonance mechanism is to say that the continental shelf tides were generated by co-oscillation with oceanic tidal waves when the oceanic tidal waves are propagated onto the continental shelves. This treatment, however, is difficult to succeed. Supposedly, the oceanic tidal waves have smoothly spread onto the continental shelf seas, but their resonances with local oscillations still aren't easy to occur as we thought, this is because the resonance of two waves has a strictly physical constraint. An approach of frequency is simply not enough. At least, the phase of two waves must be the same. For example, if the wavelengths of two sinusoidal waves are the same while phase lag between them is 180^{o}, the amplitude of the combined wave would be zero, this could be a minification of rather than an amplification. This may be illustrated with the composition of two sinusoidal waves $\sin(2\omega t)$ (the natural) and $\sin(2\omega t+k45)$ (the forced), which resemble the semidiurnal tides, the natural and the forced conceptually represent the oscillation of continental shelf sea and the oceanic tidal wave, respectively, where ω is angular speed of unit degree per hour, and $\omega = 15^{o}$, t is the time of unit hour, $k45$ is phase lag of unit degree, k=0, 1, 2, 3, 4, 5, 6, 7, and 8 (Fig. 3). It can be seen that the amplitudes of

some of these combined waves are greatly decreased when phase lag falls into a span of 135^{o}~225^{o}, in particular, the amplitude reduces to zero when phase lag is 180^{o}. The amplitudes indeed may be amplified when phase lag falls into a span of 0^{o}~135^{o} and 225^{o}~360^{o}.

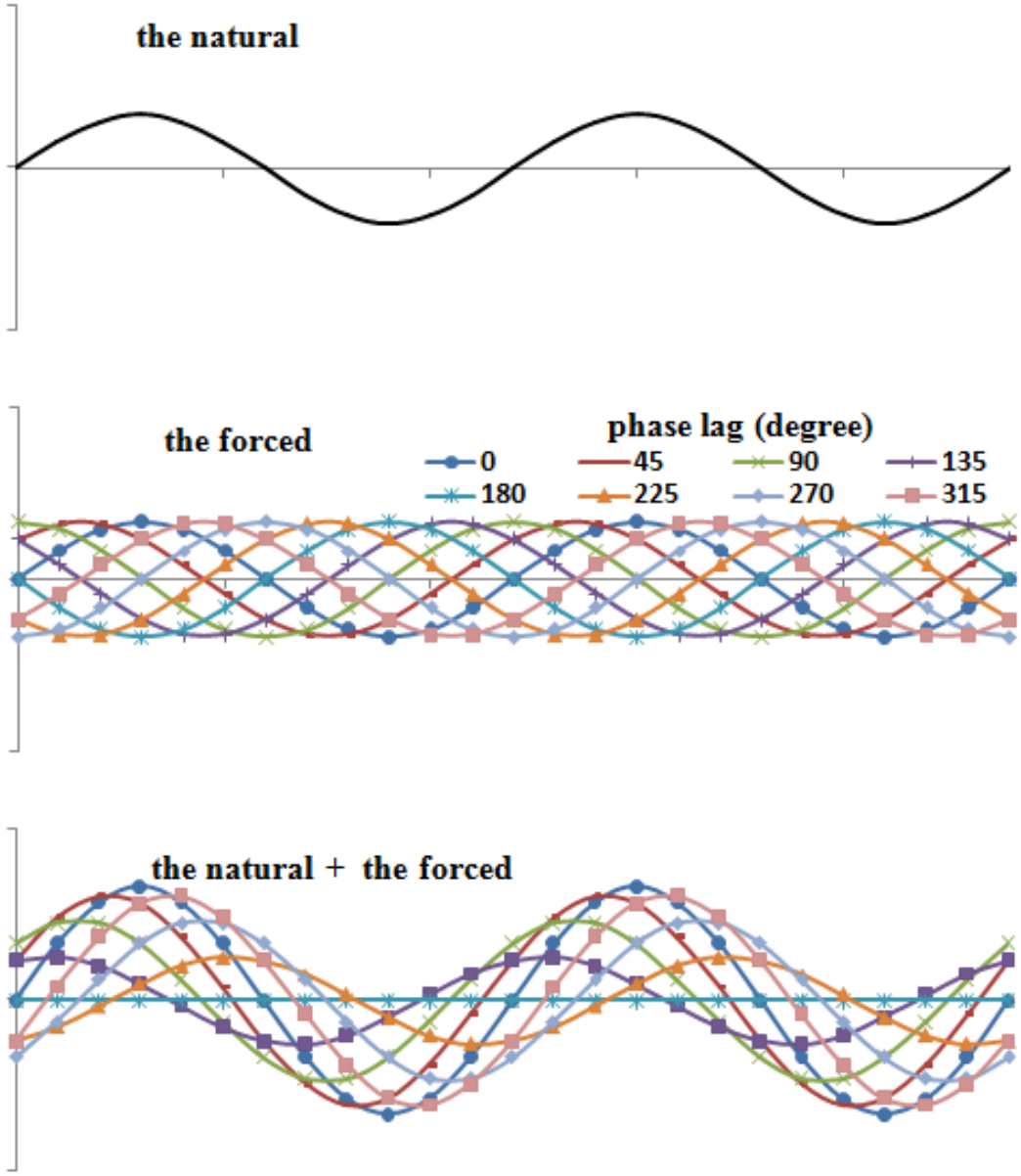

FIG. 3 Modelling the resonance of natural oscillation and forced oscillation under different phase lag.

The demonstration above leads to the fact that a system, which is forced by oscillation close to its natural period, is uncertain to yield a large amplitude anywhere. One should be aware that, due to the moon's daily advance in its orbit, the gravitational pull of the moon on an earthly site has a phase (time) lag of about 52 minutes per day (equivalent to 3.75^{o}). This means that, after 36 days the total phase lag falls into a span of 135^{o}~225^{o}, in which a counteraction of the two will occur. In other words, to maintain

the resonance between oceanic tidal wave and the oscillation of continental shelf sea, the latter has to timely recede in order to keep synchronization with the former. This hence leads to another problem why the oscillation of the continental shelf sea may recede day by day. It is unintelligible, because the natural (inherent) oscillation of a system never advances or recedes. One must also be aware that, in the real world the occurrences of resonated events (collapsing bridge, acoustic speaker, for instance) are rare, there is no eternal resonance for a special system. Attempting to relate resonance to tide seems violate our intuition.

1.3 A short description of tidal prediction

Many people (especially those engage in tidal field) mistakenly attribute the success of tidal prediction to the attractive mechanism. However, before this work is put forward further, we have to clear out this misconception. A widely accepted routine for tidal prediction is by means of tide observation. As tidal variations (the height and time of high and low waters) are recorded continuously, once tide data become available, one use computers to analyze the data to identify many components of complex wave. Tidal analysis usually employs three methods: non-harmonic, harmonic, and responsive. A detailed description of these methods may refer to the Pugh's work (1987). Historically, William Thomson devised the harmonic method about the year 1867. The principle of this method is that any periodic motion or oscillation can always be resolved into the sum of a series of simple harmonic motions. Apparently, a curve plotted from tide record may be regarded as a complex wave. As wave has crest and trough, this feature corresponds to the high and low water of a tide. Harmonic analysis makes full use of this point, by which the tidal variations (high and low) are represented with a finite number of harmonic terms of cosine form ($H_n\cos(\sigma_n t - g_n)$, where H_n is amplitude, g_n is phase lag, and σ_n is angular speed). Tidal analysis worked out the wave heights and time lags (related to the moon's or sun's orbital movement) of many components. Once the timing, periodicity, and amplitude of each component are known for a particular location, a simple addition of these components gives the tidal height at the future time at the location. In other words, by the harmonic method the calculated tide components are finally combined into a composite tide. Tidal predictions made in this way are used extensively and give the basis for the tide forecasts we daily see in many public forms (Segar 2012). From a viewpoint of the timeline of tidal prediction, before the year 1884, all tidal predictions for the tide tables were done by means of auxiliary tables and curves constructed from the results of tide observations. From 1885 to 1965, the predictions were made by means of the tide-predicting machines. These machines were superseded in 1965 by the advent of digital electronic computers of very large bulk. In the late 1980s these bulky ones were further replaced with the growing sophistication of the desktop computers. The rapid development of computers further fostered tide models when tide-gauge data and satellite altimeter data had been largely collected. Tide models are also the need for geophysical corrections in the fields such as oceanography and space technology (Provost 1994). The first generation of ocean tide models was published between 1960's ~1980's and followed by improved works in the following decades (Egbert and Erofeeva 2002; Arbic et al. 2008; Egbert et al. 2004; Hill et al. 2011; Schwiderski 1979: Eanes and Bettadpur 1996). Some comprehensive

evaluations of ocean tide models may refer to these works (Shum et al. 1997; Stammer et al. 2014). Nowadays most of tides around the world may be produced through these tide models. In these tide models, not only many different variables may be treated at a time, but also the time of data processing is greatly shortened, these wholly guarantee the decomposed tide components more reliable and the predicted tides more accurate.

Finally, we come to the conclusion that the attractive mechanism fails to account for tide and that tidal prediction cannot shield the attractive mechanism anymore. And then, if it isn't the moon's (sun's) gravitational pull to directly elevate water to form tide, a solution is needed.

For a long time, too much attention was paid to ocean tides whereas the deformation of solid earth (also called earth tide) was less considered. Love (1909) presented the first theory of solid earth deformation, Longman (1963) introduced a Green's function by which the surface deformation of the earth can be calculated exactly, these authors (Hendershott 1972; Farrell 1973; Melchior 1974; Agnew 1981; Scherneck 1991) systematically investigated the responses of solid earth to the tide-generating forces and to ocean tide. Along with these efforts, it is established that the deformation of solid earth follows the shape of the equilibrium tide. However, once the two bulges of water and the depression, which represent the equilibrium tide, is refused, the reality of the deformation of solid earth needs to be revalidated. In doing so, we use gravity data of 9 globally distributed gauge sites to analyze their responses to the lunar angles. The result agrees to the existence of the deformation of solid earth. As shown in Figure 1(C), these gauge sites commonly perform a fall of gravity when their lunar angles fall into a phase of 0^o~45^o and 135^o~180^o, but perform a rise of gravity when their lunar angles fall into a phase of 45^o~135^o. The fall (rise) of gravity geographically represents a rise (fall) of elevation relative to the earth's centre. These sites are highly scattered on several continents. This closely response of gravity to lunar angle, if we refer to Figure 1(A), quite fits to a frame of the two bugles of solid earth and a depression of solid earth around the earth halfway between the two bulges. The chart exhibits a state of 24 hours in the day of August 13, 2014. Gravity data are treated as follows: gravity change of a site is the difference of the mean of all hourly gravity changes of this site during the whole August and the hourly gravity change. This eventually yields a same reference frame (gravity is 0) for these data to be compared together. Solid earth covers with oceans, any deformation of solid earth has to disturb the water in the oceans. It's widely accepted that the influence of the deformation of solid earth on ocean tide is expressed with $(1+k-h)\Omega p/g$, where $\Omega p/g$ is the equilibrium tide amplitude, $(1+k-h)$ is a diminishing factor (combination of Love numbers) in the equilibrium tide (Pugh 1987; Pugh and Woodworth 2014). This treatment, however, lost something important. Since $(1+k-h)\Omega p/g$ itself represents tide amplitude, this means that the contribution of the deformation of solid earth to ocean tide is simply a reduction of tide amplitude in the vertical direction. In fact, solid earth responds quickly to the external forces. Once solid earth is deformed, the spinning deformed earth would mechanically drive each part of ocean basin to move up and down, under the effect of the earth's gravity, water in ocean basin begins to flow. For

a site of ocean basin, the inflow of water increases water level whereas the outflow of water decreases water level, tide therefore occurs.

2 An analytic treatment of solid earth deformation

The earth may be treated as a solid sphere that is enveloped by water and atmosphere (Fowler 2004; National Research Council 1964, 1993). The structure of solid earth, from surface to interior, is sequentially divided into different layers like crust, mantle, outer core, and inner core (Jordan 1979). A large number of works had confirmed that these layers are filled with various materials (Wootton 2006; Stixrude and Cohen 1995; Ozawa et al. 2011; Herndon 1980; Herndon 2005; Birch 1964) and denser materials are concentrated towards the interior (Monnereau et al. 2010). Notwithstanding, solid earth is strictly not a rigid body. Both experiment and measurement had proved it to be elastic (Stixrude and Cohen 1995; Schettino 2014) and to had been stretched into an oblate spheroid because of the centrifugal effect of the earth's rotation about its axis (Heiskanen 1962; Burša 1993). It has been already established that there are two curved motions for the earth in space: one is the earth orbits about the centre of mass of the earth-moon system, and another is the earth-moon system orbits about the sun. Fuller details of these motions of the earth, moon, and sun may be found in these works (Kopal 1969; Schureman 1976; Smart 1940; Doodson and Warburg 1941; Kaula 1968; Roy 1978). These two curved motions generate two centrifugal effects F_1 and F_2 for solid earth (Fig. 4(a_1)). F_1 and F_2 are mechanically balanced by the gravitation f_1 from the moon and by the gravitation f_2 from the sun. The ratio of F_1 and F_2 will be 1:178 according to some established parameters such as orbital radius and period, mass of each body, and so on. Apparently, F_2 is far greater than F_1, but because its working point is not at the earth's centre, we thus suppose the effective part of F_2, which is able to stretch the earth, to be relatively small and to exert at the earth centre. The counteraction of F_1 (F_2) and f_1 (f_2) elongates solid earth along the earth-moon (sun) line and compresses it in the midway of the elongation, the net effect is solid earth becomes an oblate spheroid (Fig. 4(a_2 and a_4)). We call these lunar (solar) deformation in the following sections. A rigorous dynamically treatment on this matter may refer to Pugh's work (1987, pp60-63). We finally see, solid earth undergoes two sets of deformations at the same time. This determines that the position of any earthly site with respect to the earth's centre is a consequence of the combination of these two sets of deformations. Since a section which cuts an oblate spheroid along its long axis would form an ellipse (Fig. 4(a_3 and a_5)), and thus, according to the geometry of ellipse, the vertical displacement of an earthly site M relative to the earth's centre at time t may be expressed as

$$\Delta H_{(t)} = \Delta H(lunar)_{(t)} + \Delta H(solar)_{(t)}$$
$$\Delta H(lunar)_{(t)} = [(R+k_m)^2\cos^2\alpha + (R-k_m)^2\sin^2\alpha]^{1/2} - R$$
$$\Delta H(solar)_{(t)} = [(R+k_s)^2\cos^2\beta + (R-k_s)^2\sin^2\beta]^{1/2} - R \quad (1)$$

Where $\Delta H(lunar)_{(t)}$ and $\Delta H(solar)_{(t)}$ are respectively the vertical displacement of site M in the lunar and solar deformations. R is mean radius of solid earth, k_m and k_s denote the amplitude of the lunar and solar deformation. α and β are the lunar and solar angle of site M, they may be calculated through these formulas of spherical geometry: $\cos\alpha = \sin\sigma\sin\delta_m + \cos\sigma\cos\delta_m\cos C_{mm}$, $\cos\beta = \sin\sigma\sin\delta_s + \cos\sigma\cos\delta_s\cos C_{ms}$,

where σ, δ_m, δ_s, C_{mm}, and C_{ms} are respectively the geographic latitude of site M, the declination of the moon, the declination of the sun, the hour angle of site M with respect to the moon, and the hour angle of site M with respect to the sun.

The expression above allows the assumption that the elongation and depression for each set of deformation keep equal in amplitude, and indicates that the vertical displacement $\Delta H_{(t)}$ is relevant to the angles α and β, this further means that site M would regularly rise and fall as the earth spins. The amplitudes of the rise and fall vary with the adjustment of the relative positions of the moon, sun, and earth, in particular, they becomes maximum at the times of full and new moon and minimum at the times of first quarter and last quarter. This is because at the times of full and new moon the two sets of deformations add each other to reinforce, whereas at the times of first quarter and last quarter the two cancel each other to weaken. A closely coupling of gravity and lunar angle, as shown in Figure 1(C), suggests this relation may be used to determine the deformation amplitude $k_m(k_s)$. Gravitation acceleration at an earthly site fits to an expression $g_H = GMe/H^2$, the resultant gravity change would be $\Delta g = (1/H^2\text{-}1/R^2)GMe$ when $g = GMe/R^2$ is referred, where G, Me, R, and H are respectively gravitation constant, mass of the earth, mean radius of the earth, and the distance of the site from the earth's centre, which, refer to equation (1), may be further written as $H = [(R+k_m)^2\cos^2\alpha + (R-k_m)^2\sin^2\alpha]^{1/2} + [(R+k_s)^2\cos^2\beta + (R-k_s)^2\sin^2\beta]^{1/2} - R$. A purely experienced treatment for these two sets of deformations would be $k_m = E_m Q_m(\cos\delta_m + \cos\Theta)$ and $k_s = Q_s\cos\delta_s$, where E_m is elliptical coefficient of the moon's orbit and may be written as $E_m = R_{ME}^2/R_M^2$ (R_{ME} and R_M denotes respectively the mean distance of the moon from earth and the orbital radius of the moon), this influences the gravitational force f_1 from the moon and the centrifugal effect F_1, Q_m and Q_s denote the amplitudes of the lunar and solar deformations, δ_m, Θ, and δ_s denote respectively the moon's declination, the angle of the moon and sun, and the sun's declination. After these parameters are packed together, we employ a set of hourly gravity data of 4 sites (which cover the whole August of 2014), by means of a regression analysis, to get Q_m and Q_s. As each gravity gauge site involved has its own reference level g_{re} when measurement is operated, the gravity change of a site may thus be expressed as $\Delta g = (1/H^2\text{-}1/R^2)GMe - g_{re}$. The calculated and measured gravity changes are compared in Figure 5, the values of related parameters (G, Me, R, and R_{ME}, for instance) that bear these calculations and the results for Q_m, Q_s, and g_{re} are listed in Table 1.

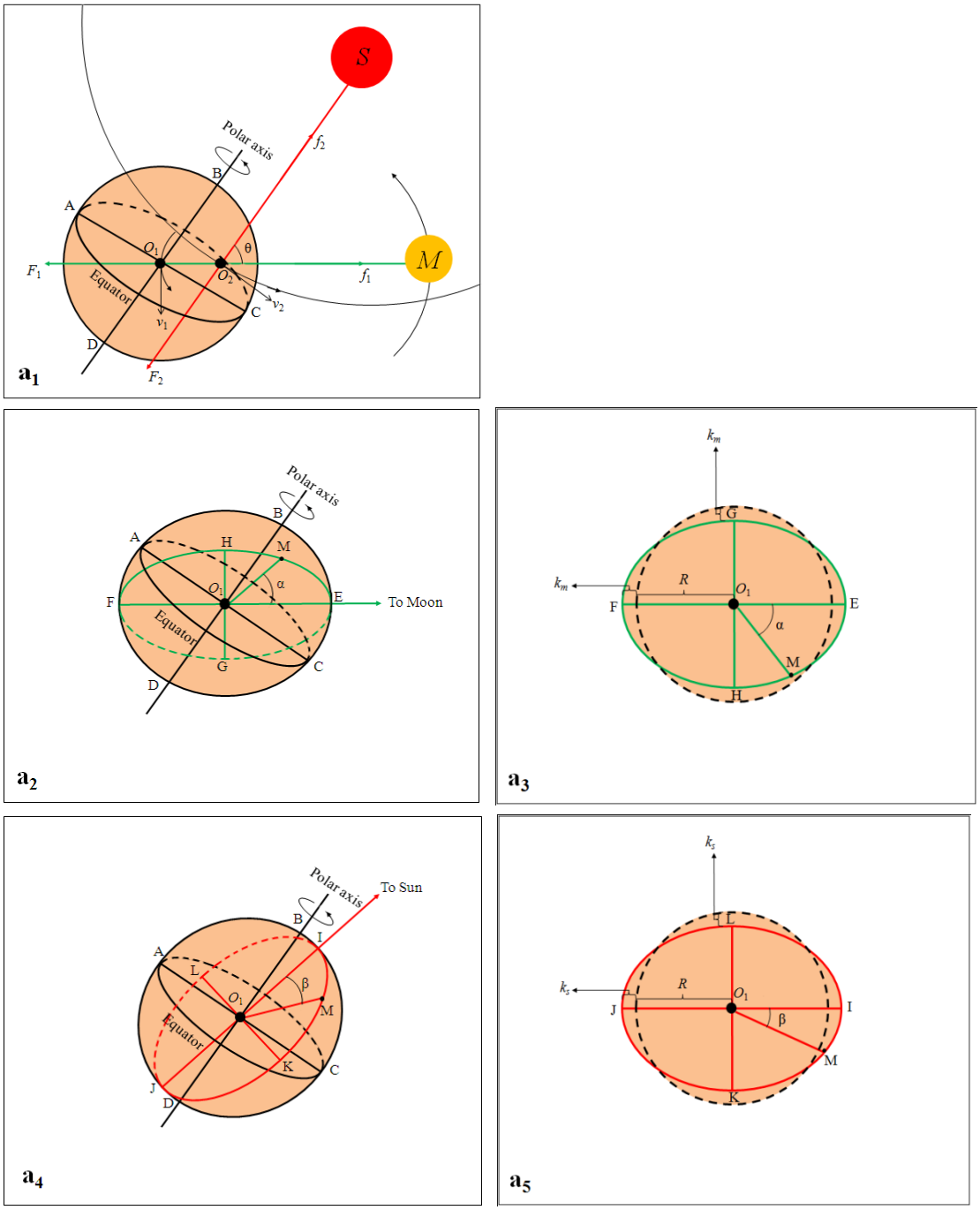

Fig. 4 Combined centrifugal effects for solid earth and the resultant deformation. a_1, the curved motions of the earth around the barycenter of the earth-moon system and around the sun, a_2 and a_4 are the resultant deformations respectively from the moon and from the sun, a_3 and a_5 are the elliptical intersections respectively from these deformations. F_1 and F_2 are the centrifugal effects solid earth undergoes due to these curved motions. O_1, O_2, M, and S are the earth's centre, the barycenter of the earth-moon system, the moon, and the sun, respectively. Θ is the angle of the moon and sun relative to the barycenter of the earth-moon system. v_1 and v_2 are respectively the velocity of the earth orbiting the barycenter of the earth-moon system and the velocity of the earth-moon system orbiting the sun, it is these motions to generate the centrifugal effects F_1 and F_2. Black dashed circles in diagram a_3 and a_5 are referred as the original shape of solid earth.

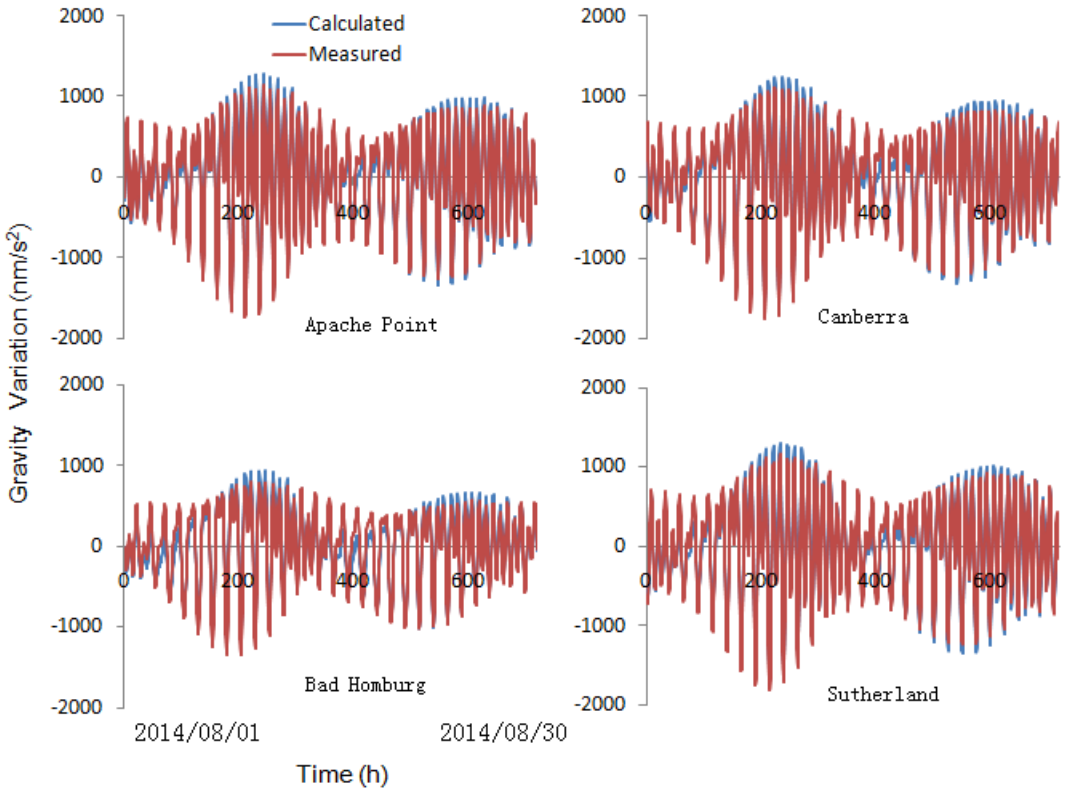

FIG. 5 Comparison of calculated and measured gravity change. Gravity data refer to IGETS (International Geodynamics and earth Tide Service) (Voigt et al. 2016).

Table 1 Parameters and results calculated for lunar and solar deformations

Astronomical parameters	Moon	M_m	$7.35*10^{22}$ kg (Wieczorek et al, 2006)			
		R_{ME}	384400 km (Wieczorek et al, 2006)			
	Earth	M_e	$5.97*10^{24}$ kg (Luzum et al., 2011)			
		R	6370 km (Lide, 2000)			
	Sun	R_s	$1.49*10^{8}$ km (Simon et al., 1994)			
		M_s	$1.99*10^{30}$ kg (Williams, 2013)			
	G gravitational constant		$6.67\times10^{-11}m^3kg^{-1}s^{-2}$			
Geographic sites	Name		Apache Point, New Mexico, USA	Bad Homburg, Germany	Canberra, Australia	Sutherland, South Africa	Mean
	Latitude		32.78°N	50.23°N	35.32°S	32.38°S	--
	Longitude		105.82°W	8.61°E	149.01°E	20.81°E	--
Calculated	Q_m (m)		0.19	0.18	0.19	0.19	0.19
	Q_s (m)		0.11	0.12	0.11	0.11	0.11
	g_{re} (nm/s^2)		379.04	695.91	426.76	371.88	--

Note: Q_m, Q_s, and g_{re} are respectively the amplitudes of the lunar and solar deformations, and gravity reference level of each site. M_m, M_e, and M_s are respectively the moon's, the earth's, and the sun's mass; R earth's mean radius, R_{ME} and R_s are respectively the mean distance of the moon from the earth and

the mean distance of the sun from the earth.

3 An ocean basin oscillation-driving mechanism for tide

Our understanding of tide begins with a demonstration of the water movement in an oscillating vessel. As shown in Figure 6, we firstly let the right end of a rectangular water box rise, the water then flows towards left. If line MN represents reference level, the water level at site M rises whereas the water level at site N falls. We restore the right end of the vessel to its former level and continue to let the left end rise, the water at the left end flows towards right, the water level at site M correspondingly falls whereas the water level at site N rises. Repeat the rise and fall of the two ends continuously, the water level of sites M and N alternately vary. Compared to sites M and N, another site S, which is located in the middle of this vessel, always holds a minimal variation of water level. Now we let only one end rise and fall alternately, the water level at sites M and N still alternately vary. Further, we let one end rise (fall) but another end fall (rise) at the same time, the water level at sites M and N also alternately vary. The variation of water level at one end may be approximately expressed with a difference of vertical displacement between the two ends, i.e., $\Delta H=H_N-H_M$, where H_N and H_M denote respectively the vertical displacement of sites N and M. Mathematically speaking, this variation may be depicted with a sinusoidal function *of* $h\sin(\omega t+\sigma)$, where h, ω, and σ denote respectively amplitude, angular frequency, and phase lag. It should be noted that, this mode is different from the first gravitational mode of the oscillations of water that was mentioned in the Pugh's work (1987, pp149), in that gravitational mode the vessel remains motionless and the oscillations of water are ascribed to a pull of tide-generating force.

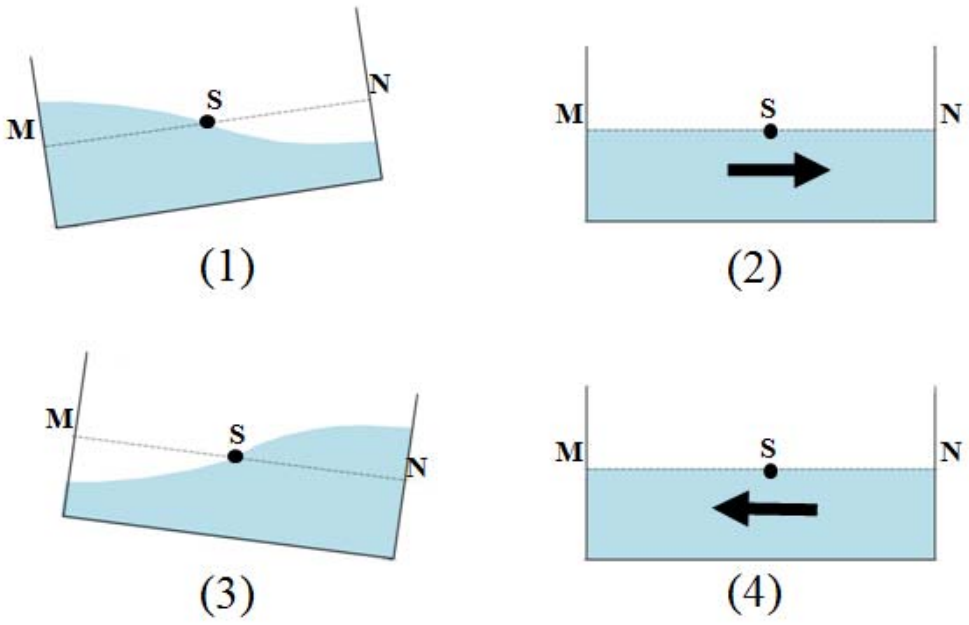

FIG. 6 Modelling the water movement of an oscillating rectangular box. From (1), (2), (3) to (4) it orderly represents a full alternation of the rise and fall of the two ends. Arrows denote the directions of water movements.

Go back to real world, about 71% the earth's surface is covered with ocean (Pidwirny 2006). Apparently, ocean basin looks like a gigantic vessel of water. In consideration of the matter of solid earth deformation we consider above, the spinning earth would have to drive every part of ocean basin to regularly rise and fall, this leads water to flow between all the parts of ocean basin, and thus generates high and low water variation at each of these parts. The water transferring may be roughly outlined with Figure 7. Within the lunar deformation, the elongated solid earth is represented with two bulges in the direction of the earth-moon line, these two bulges track from east to west along line *L* and *L*' as the earth spins, this leads ocean basin to oscillate (i.e., rise and fall) and subsequently gives birth to a flow of water between all the parts of the basin. As the inflow of water would result in an increase of water level, whereas the outflow would result in a decrease of water level, this ultimately gives a site two high and two low waters during a lunar day when the two bulges are included. This oscillation of ocean basin, which is generated by the lunar deformation, is added to another oscillation of ocean basin, which is generated by the solar deformation, the resulting two sets of water transferring becomes strongest at the times of full and new moon and weakest at the times of first quarter and last quarter, this generates two cycles of high and low waters during a lunar month. Finally, the water level variation of a site is the composition of the water level variations of all sites in the ocean basin.

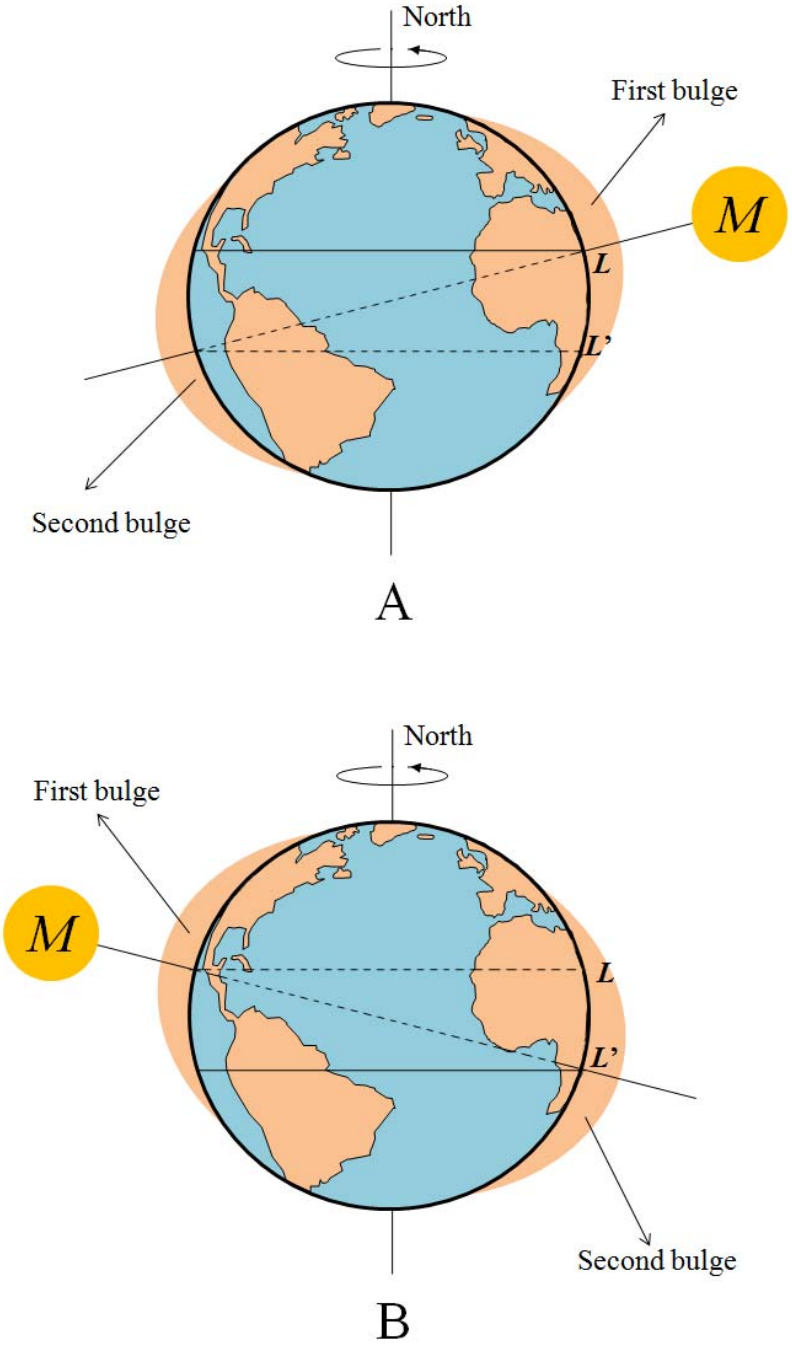

FIG. 7 A simplified system illustrates the spinning deformed solid earth. From A to B, the earth rotates 180^{o} with respect to the moon. *L* and *L'* denote the paths that the earth-moon line tracks along the earth's surface (dashed line means it is at far side), the two bulges represent the elongation of solid earth.

Once ocean basin is treated as a vessel of water, also because ocean water is globally conservative, the water level variation of a site within ocean basin would be a consequence of the combination of the water level variations of all other sites. To

support the following model, we divide the globe into a grid of $15^{o}*15^{o}$ and use the locations of nodes of the grid, which are situated in the ocean basin, to act as oscillators (Figure 8), and then, the model for the water level variation of a site at time t may be approximately expressed as

$$\Delta Y_{(t)} = \sum_{i=1}^{n}\sum_{j=1}^{k} Qa_i b_j\left(lunar\right)\Delta Ha_i b_j\left(lunar\right)_{(t)} + \sum_{i=1}^{n}\sum_{j=1}^{k} Qa_i b_j\left(solar\right)\Delta Ha_i b_j\left(solar\right)_{(t)}$$
$$+Q_s\left(lunar\right)\Delta H_s\left(lunar\right)_{(t)} + Q_s\left(solar\right)\Delta H_s\left(solar\right)_{(t)} \qquad (2)$$

where $\Delta Ha_ib_j(lunar)_{(t)}$ and $\Delta Ha_ib_j(solar)_{(t)}$ are respectively the vertical displacement of a_ib_j oscillator in the lunar and solar deformations at time t, n=24 and k=11, referring to the map, combine together to represent the number of oscillators. $\Delta H_s(lunar)_{(t)}$ and $\Delta H_s(solar)_{(t)}$ are respectively the vertical displacement of the site itself in the lunar and solar deformations at the time. These vertical displacements may be got based on equation (1). $Qa_ib_j(lunar)$, $Qa_ib_j(solar)$, $Q_s(lunar)$, and $Q_s(solar)$ are the coefficients of oscillations of all related sites.

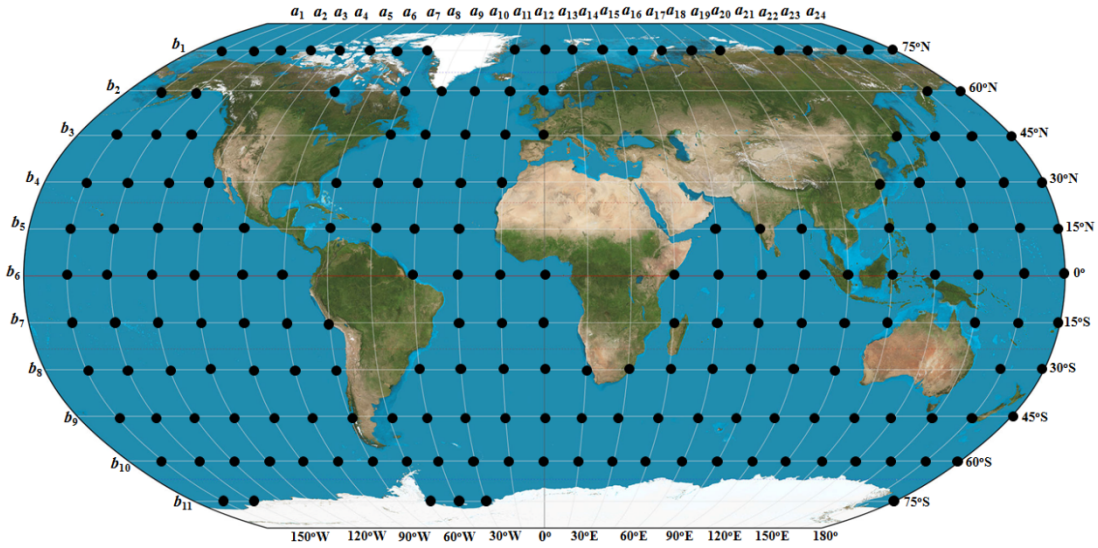

FIG. 8 A globally-distributed oscillators within ocean basin. The background image is created by Daniel R. Strebe with the Geocart map projection software.

About 187 oscillators are extracted from the nodes of the grid that covers ocean basin, the grid is plotted referring to both equator and meridian, this makes the geographic latitude and longitude of these oscillators easily known from the map. The behaviour of these oscillators is similar to that of the constituents of the harmonic analysis. The hourly tide-gauge data lasting the whole August of 2014 from 75 UHSLC stations are used to test the model. The evaluation of the results are realized in terms of the *RMS* deviation of amplitude and the Root Sum of Squares (*RSS*). The *RMS* deviation for a tide-gauge site during the month may be written as

$$RMS = \sqrt{\frac{\sum_{i=1}^{m}\left(\Delta Y_{(t)-calculated} - \Delta Y_{(t)-observed}\right)^2}{mp^2}} \tag{3}$$

where $\Delta Y_{(t)\text{-}calculated}$ and $\Delta Y_{(t)\text{-}observed}$ denote respectively the in-phase amplitudes of the calculated and tide-gauge data, and m=744, which denotes a time sequence of 31 days multiply 24 hours during the month, and p=376, which is the total number of the oscillations (including the 187 oscillators and the tide-gauge site itself) in the lunar and solar deformations.

The Root Sum of Squares (*RSS*), reflecting a total effect of the p oscillations for the model against the observations at a tide-gauge station, is calculated by

$$RSS = \sqrt{(\sum_{i=1}^{p} RMS^2 p)} = RMS\sqrt{p} \tag{4}$$

The results for 78 UHSLC tide-gauge stations in terms of *RMS* and *RSS* are shown in Table 2, some of the calculated and tide-gauge data are compared in Figure 9. These fittings strongly agree that the observed tides may be a consequence of the oscillation of ocean basin. It should be noted, we cannot use a comparison of the *RSS* to simply conclude that the model presented here is better than the established ocean tide models (NSWC, CSR3.0, HIM, OTIS-GN, STM-1B, HYCOM, OSU12, HAM12, for instance). A critical reason for this point is the model presented here employs 376 oscillations (similar to 376 constituents), whereas the established tide models often include eight major constituents (M_2, S_2, N_2, K_2, K_1, O_1, P_1, and Q_1), the number the constituents of a model technically controls the value of the *RSS*. Nevertheless, the *RMS* would be available. The total *RMS* of the p oscillations of the model presented here may be written as

$$TRMS = pRMS = \sqrt{\frac{\sum_{i=1}^{m}\left(\Delta Y_{(t)-calculated} - \Delta Y_{(t)-observed}\right)^2}{m}} \tag{5}$$

The average of the *TRMS* estimated for deep ocean (34 sites) and shelf-coastal regions (41 sites) is respectively 6.16 and 10.27 cm. The *TRMS* of the established ocean tide models is deduced from the *RSS*. According to Stammer et al. (2014), the *RSS* of the eight major constituents of the best ocean tide model are approximately 0.9, 5.0, and 6.5 cm for pelagic, shelf, and coastal conditions, therefore, the *TRMS* of the established tide models can be calculated by $2^{3/2}RSS$, the values estimated are 2.55, 14.14, and 18.39 cm, respectively. And then, the model presented here is excellent in dealing with shelf-costal tides than the established tide models.

Of course, the model presented here is not limited in the fitting of tide observations, one of its functions is to provide new way for making tide prediction. Simply, it takes the tide-gauge data using a regression analysis to firstly solve the coefficients of these oscillations involved, and then, each of these known coefficients are further used to multiply the vertical displacement of its corresponding oscillation at the future time, a tidal height for each oscillation is therefore got, subsequently, a simple addition of

these tidal heights gives the total tidal height at the location at the future time. We take the hourly tide-gauge data of the whole August of 2014 to make tide prediction for the following month (September 2014) and find that the prediction is successful for some of the 75 sites we selected above. Figure 10 compares the tide predictions of four sites (Atlantic city, San Francisco, Adak, and Betio) with the observations. The evaluation of these predictions is made through the Root Mean Square (*RMS*) (the difference of prediction and observation) to estimate the average errors. The calculated *RMS*s for these sites are 16.36, 15.47, 16.79, and 19.78 cm, respectively. It may be safe to say, relative to the tide range of each site during the month, such an accuracy of tide prediction could be effective for the activities of living practice. The improvement of this model and its resultant prediction should be focused on two aspects: 1) the globe may be divided into smaller grid of 5^o*5^o or 1^o*1^o, this helps to add more oscillators into the model. We believe, more oscillators that are added to the model, and more accurate the model will become. It should be noted, a well-equipped computer and powerful software should be prepared for the addition of oscillator. This model uses a computer of CPU 3.40 GHz and RAM 16.0 GB) with a software (1stOpt-First Optimization, 7.0 version) to work, but not too satisfactory, each round of regression analysis takes too much time; and 2) a longer tide-gauge data record of a few months or one year should be considered to resolve the coefficients of oscillations of the model so as to enhance the accuracy of tide prediction. A merit of this model is the time lag of tide is unnecessary to be considered, but for a more exactly prediction, the influences of these factors such as the shape of ocean basin, orientation of coastline, water depth, Coriolis effect, inertia, and so on, must be considered. Since water level variation of a site is a consequence of the combination of the water level variations of all parts of ocean basin, along with the influences of Coriolis force and geographic factors, these gives diversity to the times of high and low waters of all sites around the globe.

Table 2 RMS and RSS calculated for various sites over different regions

Tide-gauge station					RMS (cm)	RSS(cm)
ID at UHSLC	Name	Latitude	Longitude	Region		
1	Betio (Tarawa)	1.35	172.92	D	0.02	0.35
3	Baltra	0.43	269.72	D	0.04	0.83
5	Majuro	7.10	171.37	D	0.02	0.47
7	Malakal	7.33	134.47	D	0.02	0.36
8	Yap	9.52	138.13	D	0.02	0.33
14	French Fr Shall	23.87	193.72	D	0.01	0.17
15	Papeete	-17.53	210.43	D	0.01	0.12
16	Rikitea	-23.13	225.05	D	0.01	0.24
22	Easter	-27.15	250.55	D	0.02	0.38
23	Rarotonga	-21.20	200.22	D	0.01	0.25
24	Penrhyn	-8.98	201.95	D	0.01	0.14
29	Kapingamarangi	1.10	154.78	D	0.01	0.23
31	Nuku	-8.93	219.92	D	0.02	0.46

38	Nuku' alofa	-21.13	184.83	D	0.02	0.43
39	Kodiak	57.73	207.48	S	0.04	0.81
40	Adak	51.87	183.37	S	0.03	0.50
41	Dutch	53.90	193.50	S	0.03	0.66
43	Palmyra	5.87	197.90	D	0.01	0.19
46	Port Vila	-17.77	168.30	D	0.01	0.24
47	Chichijima	27.10	142.18	S	0.01	0.19
49	Minamitorishima	24.30	153.97	D	0.02	0.47
50	Midway	28.22	182.63	D	0.01	0.16
51	Wake	19.28	166.62	D	0.01	0.21
52	Johnston	16.75	190.48	D	0.01	0.15
53	Guam	13.43	144.65	D	0.01	0.20
55	Kwajalein	8.73	167.73	D	0.01	0.26
56	Pago	-14.28	189.32	D	0.02	0.31
58	Nawiliwili	21.97	200.65	D	0.01	0.16
60	Hilo	19.73	204.93	D	0.01	0.19
71	Wellington	-41.28	174.78	D	0.03	0.60
72	Bluff	-46.60	168.33	D	0.04	0.81
79	Chatham	-43.95	183.43	D	0.03	0.50
80	Antofagasta	-23.65	289.60	SC	0.02	0.37
81	Valparaiso	-33.03	288.37	SC	0.02	0.39
83	Arica	-18.47	289.67	SC	0.02	0.38
88	Caldera	-27.07	289.17	SC	0.02	0.39
91	La	-2.20	279.08	SC	0.03	0.51
93	Callao	-12.05	282.85	SC	0.01	0.27
94	Matarani	-17.00	287.88	SC	0.01	0.28
101	Mombasa	-4.07	39.65	SC	0.04	0.72
103	Port Louis	-20.15	57.50	SC	0.01	0.20
105	Rodrigues	-19.67	63.42	D	0.01	0.24
108	Hulhule	4.18	73.53	D	0.01	0.20
109	Gan	0.68	73.15	D	0.01	0.21
115	Colombo	6.97	79.87	SC	0.01	0.18
119	Djibouti	11.60	43.15	SC	0.02	0.39
121	Point La Rue	-4.67	55.53	D	0.02	0.33
122	Sibolga	1.75	98.77	SC	0.01	0.25
124	Chittagong	22.23	91.83	SC	0.11	2.04
125	Prigi	-8.28	111.73	SC	0.02	0.45
126	Jask	25.63	57.77	SC	0.03	0.54
128	Thevenard	-32.15	133.63	SC	0.04	0.81
142	Langkawi	6.43	99.75	SC	0.02	0.39
147	Karachi	24.80	66.97	SC	0.03	0.66
149	Lamu	-2.27	40.90	SC	0.03	0.61
211	Ponta Delgada	37.73	334.32	SC	0.02	0.36
223	Dakar	14.70	342.60	SC	0.02	0.37

235	Palmeira	16.70	337.00	D	0.01	0.21
245	San Juan	18.47	293.88	SC	0.01	0.17
253	Newport	41.50	288.67	SC	0.03	0.49
257	Settlement Point	26.72	281.00	SC	0.02	0.34
259	Bermuda	32.37	295.30	D	0.02	0.38
260	Duck Pier	36.18	284.27	SC	0.03	0.50
264	Atlantic City	39.40	285.00	SC	0.03	0.55
276	St-John's	47.57	307.28	SC	0.02	0.41
299	Qaqortoq	60.70	314.00	SC	0.04	0.76
329	Quarry Bay	22.30	114.22	SC	0.02	0.46
340	Kaohsiung	22.62	120.28	SC	0.01	0.29
540	Prince Rupert	54.32	229.67	SC	0.07	1.39
551	San Francisco	37.80	237.53	SC	0.03	0.50
752	Fort Pulaski	32.03	279.10	SC	0.05	0.95
755	Virginia Key	25.70	279.90	SC	0.02	0.38
776	Punta Cana	18.50	291.62	SC	0.01	0.16
803	Rorvik	64.87	11.25	SC	0.03	0.58
820	Nuuk	64.17	308.28	SC	0.05	1.06

Note: D, Deep ocean; SC, Shelf and Coastal area.

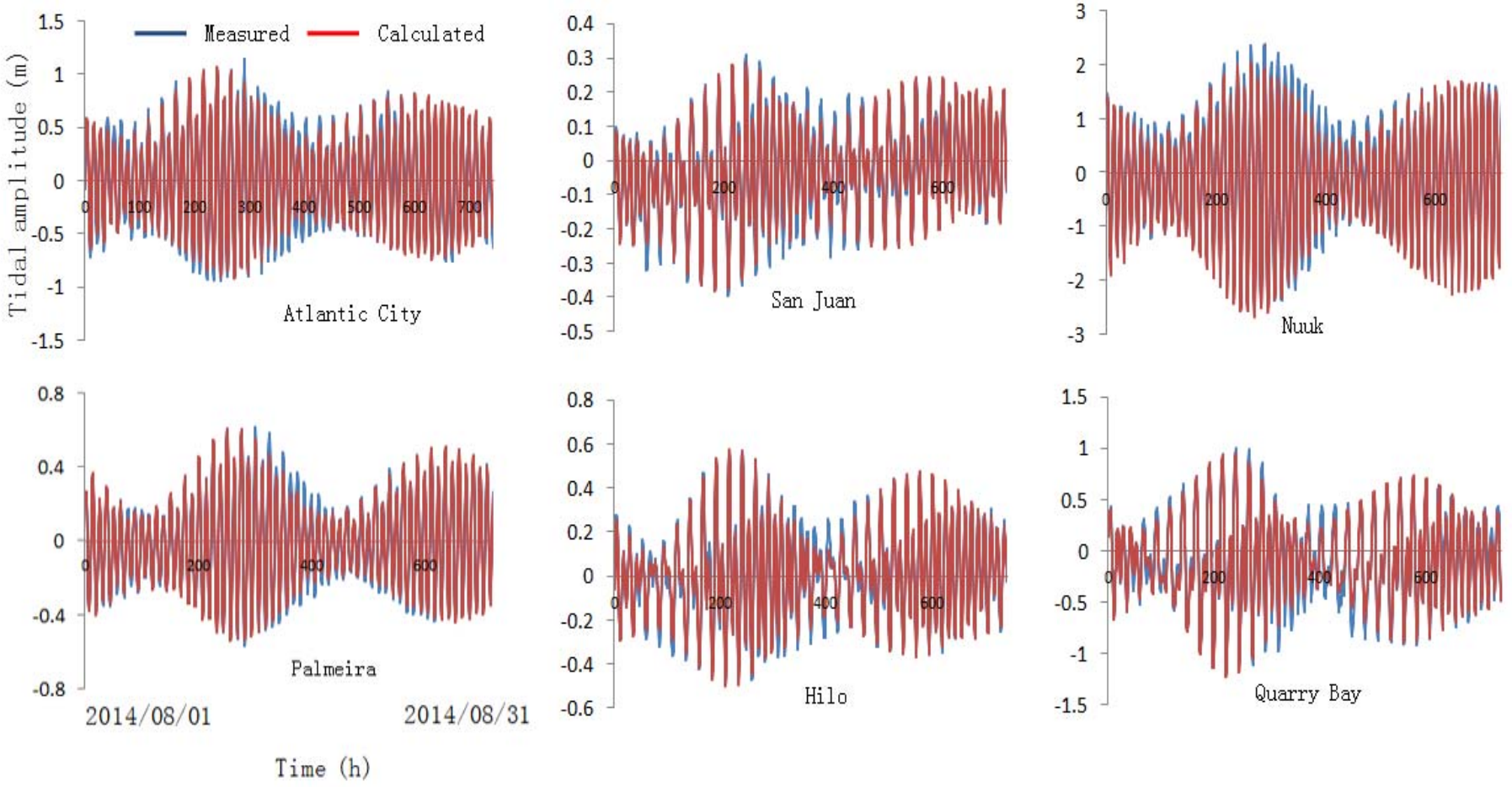

FIG. 9(A) Representatives of the comparison between the calculated and tide-gauge data covering the whole August of 2014.

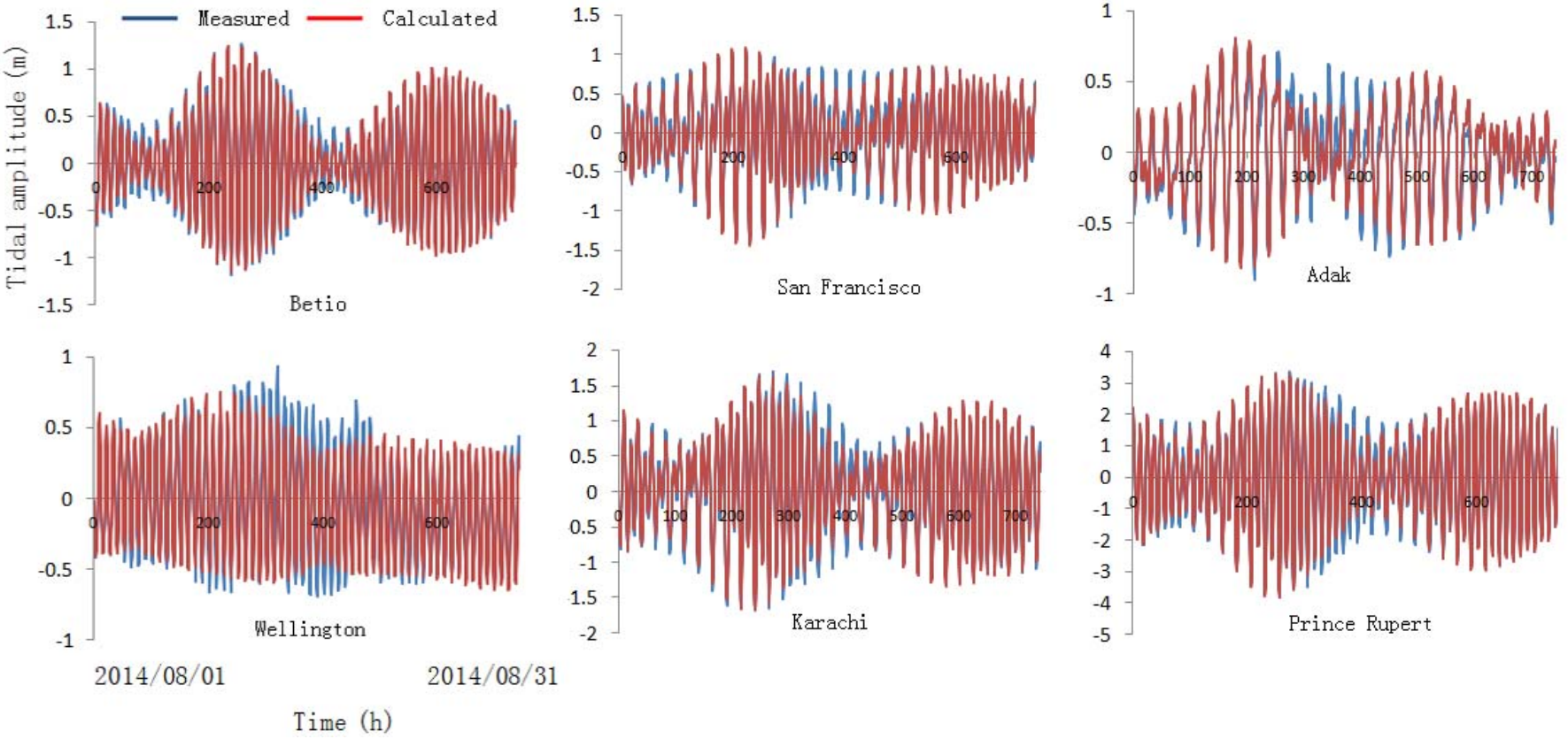

FIG. 9(B) Representatives of the comparison between the calculated and tide-gauge data covering the whole August of 2014.

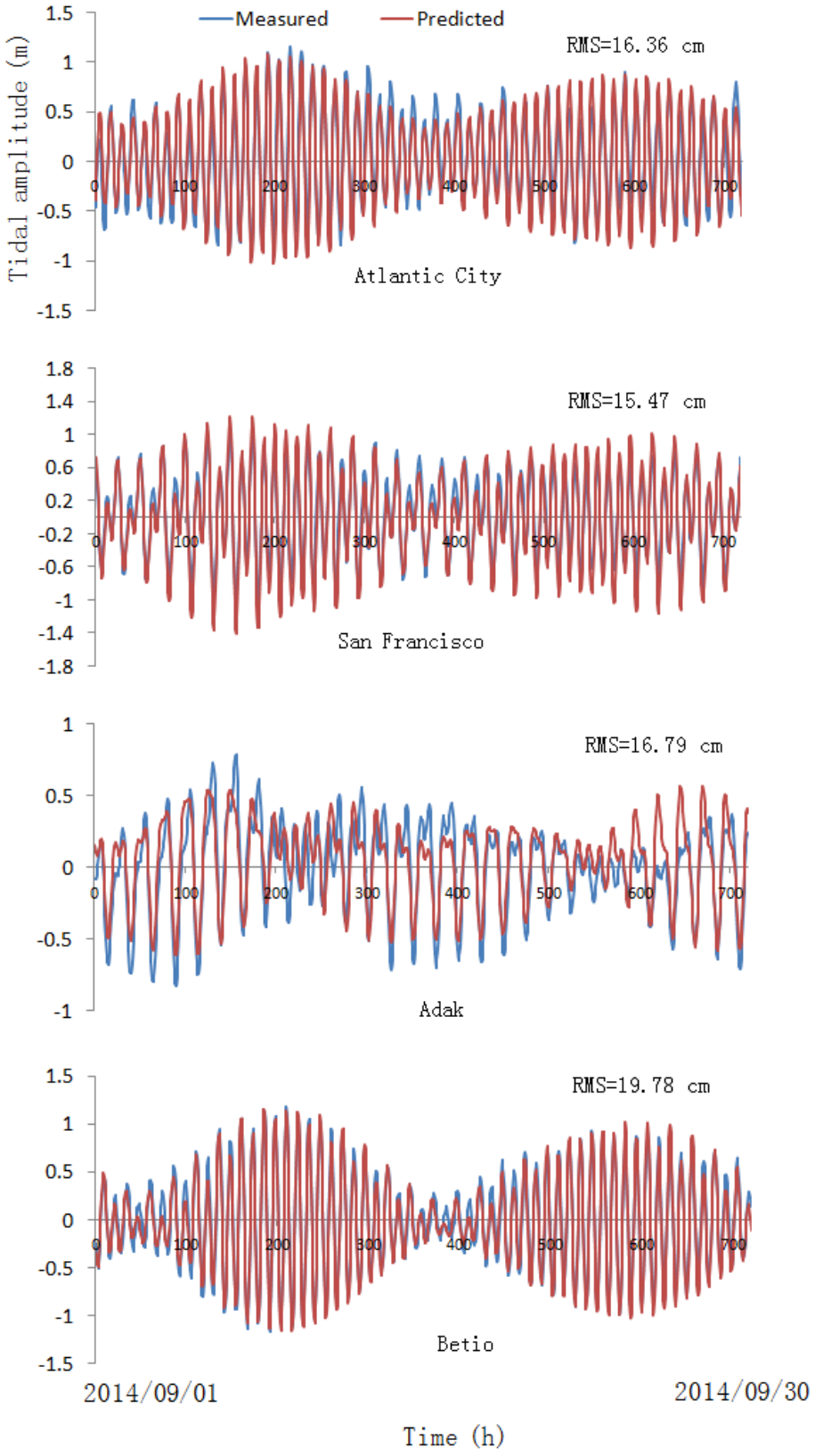

FIG. 10 A comparison of the predicted and tide-gauge data over the whole September of 2014.

4 Discussion

The physics of the oscillating vessel is also applicable to the matter of an enclosed sea/lake. If we treat Black sea as a vessel and use the model we presented in section 3 to estimate, the west or east end of this region may experience a tide of up to 17.0 cm. Similarly, a tube of water (20 m in length) horizontally located at equator will experience a tide of up to $3.2*10^{-3}$ mm, an imperceptible amount. This means that, any smaller vessel, such as swimming pool, cup, bowl, and so on, because of its short size, wouldn't exhibit a perceptible tide. The oscillating ocean basin drives water to flow back and forth, the continental shorelines are generally long enough to block the transferring water to form large accumulation. In particular, most of the shorelines are concave, this may create an effect of narrow to amplify tide. Typical representatives of this amplification could be the tides around Qiantang River and at Bay of Fundy. In contrast, the shorelines of the islands that are isolated in the deep oceans are short, the transferring water can't be effectively accumulated and may bypass. These cause larger tidal ranges to occur at the coastal seas and smaller ones to occur at the deep oceans. The transferring water, if constrained by the narrowness of a strait, may form a swift current, like that in the Cook Strait (Stevens et al. 2012; Bowman et al. 1983). For the various features of the tides in the Atlantic and in the North West Europe shelf seas, they may be understood as follows: since the rise and fall of each part of the ocean basin is launched from east to west as the earth spins, the rising of east end of the Atlantic basin first leads water to flow towards north, west, and south, the following rise of middle part of the basin leads water to flow towards east, north, west, and south, and finally, the rise of west end of the basin leads water to flow towards north, east, and south. The westerly water reaches the eastern coastline of America nearly at the same time and leaves no difference in tidal phase. The northerly water forms a progression of tidal phases oriented north in the North Atlantic. Moreover, a large body of north-easterly water may enter the strait of Gibraltar and cross the Celtic Sea, from where it continues to pass the English Channel and other related regions. A series of progressive tides along these shores are created, such as the tides around England's shores. With passage of time, the Atlantic ocean basin begins to fall from east to west, water is slowly restored. On the whole, the falling of the middle of the Atlantic basin would lead water to flow in. This gives rise to a progression of tidal phases towards north in the South Atlantic and towards south in the North Atlantic. However, the progression of tidal phases towards south is not as apparent as that towards north. This could be ascribed to the influences of the trumpet-shape North and South Atlantic. The width of the North Atlantic reaches 6400 km at 22^{o} N and 3500 km at 52^{o} N, similarly, the width of the South Atlantic reaches 3800 km at 5^{o} S and 5500 km at 33^{o} S. The southerly water at the North Atlantic and at the South Atlantic may be decompressed and minimize the phases as the channel becomes wider. In contrast, the northerly water at the South Atlantic and at the North Atlantic would be narrowed to amplify the phases as the channel becomes narrower.

Newton in his book *Mathematical Principles of Natural Philosophy* described a tide (Proposition XXIV. Theorem XIX, translated by Andrew Motte): "*An example of all which Dr. Halley has given us, from the observations of seamen in the port of Batsham, in the Kindom of Tunquin (presently Viet Nam), in the latitude of 25^{o}50' north. In that port, on the day which follows after the passage of the moon over the equator, the waters stagnate: when the moon declines to the north, they begin to flow and ebb, not twice, as in other ports, but once only every day: and the flood happens at the setting, and the greatest ebb at the rising of the moon. This tide increases with the declination of the moon till the 7^{th} or 8^{th} day; then for the 7 or 8 days following it decreases at the*

*same rate as it had increased before, and ceases when the moon changes its declination, crossing over the equator to south. After which the flood is immediately changes into an ebb; and thenceforth the ebb happens at the setting and the flood at the rising of the moon; till the moon, again passing the equator, changes its declination. There are two inlets to this port and the neighboring channels, one from the seas of China, between the continent and the islands of Leuconia; the other from the Indian sea, between the continent and the island of Borneo. But whether there be really two tides propagated through the said channels, one from the Indian sea in the space of 12 hours, and once from the sea of China in the space of 6 hours, which therefore happening at the 3d and 9th lunar hours, by being compounded together, produce those motions; or whether there be any other circumstances in the state of those seas, I leave to be determined by observations on the neighbouring shores."*Newton gave an explanation for this tide but without being verified. A similar tide also appears in the Australian Gulf of Carpentaria. The tide at this location reduce to zero when the moon's declination is zero, increasing to its largest values when the moon is at its greatest declination, either north or south of the equator. This kind of tide is presently called a diurnal tide. Here we demonstrate how this tide forms under the frame of the spinning deformed solid earth. As shown in Figure 11, when the moon declines to the north, since the elongation of solid earth is always in the earth-moon line and tracks from east to west, a part of the northern hemisphere of solid earth is dominantly raised at the moon's rising, this leads water to flow out and the water level at site Z falls naturally. With the passage of time, a part of the southern hemisphere is dominantly raised at the moon's setting. This leads water to flow out, at least, there is a water transferring from south to north, the water level of site Z rises naturally. When the moon declines to the south, a part of the southern hemisphere is dominantly raised at the moon's rising. This leads water to flow out, at least, there is a water transferring from south to north, the water level at site Z rises. With the passage of time, a part of the northern hemisphere is dominantly raised at the moon's setting. This leads water to flow out, and the water level at site Z falls. This eventually gives site Z one high water and one low water per day. When the moon lies at the equator, the water transferring between the northern and southern hemispheres is relatively slight, the water at site Z become nearly motionless.

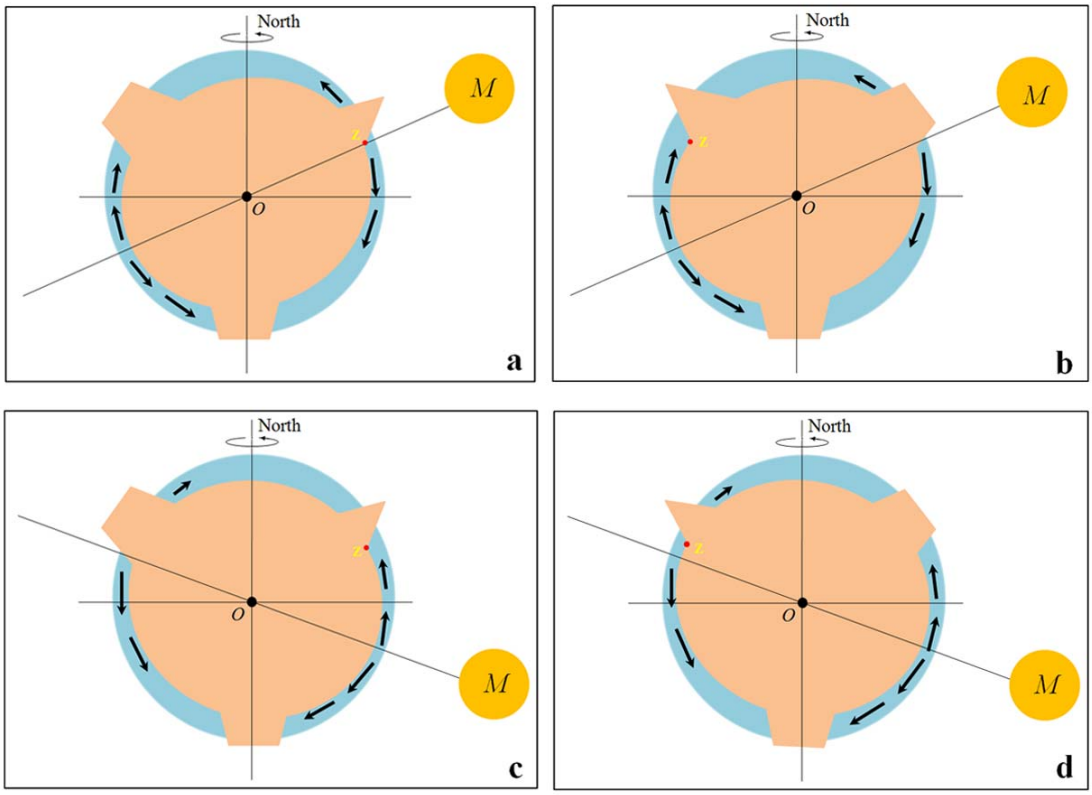

FIG. 11 Modelling the formation of diurnal tide in Batsham and Karumba (Z). From **a**(**b**) to **c**(**d**) the moon transfers from north to south. From **a**(**c**) to **b**(**d**), the earth rotates 180°. Please note, the deformation of solid earth is highly exaggerated. *M* represents the moon. Black arrows in each diagram denote water transferering caused by the deformation.

Galileo in his *Dialogue Concerning the Two Chief World Systems* (translated by Stillman Drake) described the tides of the Mediterranean, "*three varieties of these hourly changes are observed: in some places the waters rise and fall without making any forward motions; in others, without rising or falling they move now toward the east and again run back toward to the west; and in still others, the height and the course both vary. This occurs here in Venice, where the waters rise in entering and fall in departing. ... ..., elsewhere the water runs to and fro in its central parts without changing height, as happens notably in the Straits of Messina between Scylla and Charybdis, where the currents are very swift because of the narrowness of the channel. But in the open Mediterranean and around its islands, such as the Balearics, Corsica, Sardinia, Elba, Sicily (on the African side), Malta, Crete, etc., the alterations of height are very small but the currents are quite noticeable, especially where the sea is restrained between islands, or between these and the continent.*" The Mediterranean may be treated as a vessel of water. Due to the effect of the spinning deformed solid earth, the vessel is oscillated regularly, this generates water transferring between its related parts, refer to Figure 6, the greatest alternation of water level occurs at these ends, whereas the smallest one occurs in the open area. The transferring water, while constrained by the straits, form some swift currents.

A critical difference between the attractive mechanism and this proposed theory lies at, the former relates ocean tide directly to the gravitational pulls of the moon and sun on water, while the latter relates ocean tide directly to the oscillation of ocean basin; Another difference in dealing solid earth deformation (i.e., earth tide) is the former firstly treats ocean tide, and then, uses ocean tide to further multiply a diminishing

factor function (1+k-h) to express earth tide, contrary to this, the latter directly uses earth tide to account for ocean tide. We see, this proposed theory not only explains the general features of tide (the daily and fortnightly cycles of high and low waters, for instance), but also realizes some competitive results with observation, most importantly, it provides a physical foundation for presently tidal prediction. As we addressed in the section 1.3, the principle of the harmonic analysis is any periodic motion or oscillation (tide, for instance) may be treated as the addition of a series of simple motions. This treatment is relatively mathematical. For a particular site, the high water it represents is a consequence of the inflow of water from other places and the low water it represents is a consequence of the outflow of water towards other places, a simple addition of these decomposed components cannot show from where the water comes and to where the water goes. In other words, a physical foundation is necessary to explain why an addition of the decomposed components may be so. Clearly, this work has provided the answer.

Acknowledgements We thank Phil Woodworth, David Pugh, Walter Babin, Thierry De Mees, Roger A. Rydin, Duncan Agnew, and Wouter Schellart for comments on the original manuscript, we thank Hartmut Wziontek and Calvo Marta for discussions on gravity data, and we thank Mike Davis for providing tide data. We also thank these institutes (U.S. NOAA, NASA's JPL, GLOSS database - University of Hawaii Sea Level Center, Bureau National Operations Centre (BNOC) of Australia, and GGP (Global Geodynamics Project)) for their data supporting.

References

Agnew, D. C., 1981: Nonlinearity in rock - Evidence from earth tides. *J. geophys. Res.*, **86**, 3969-3978.

Arbic, B. K., J. X. Mitrovica, D. R. MacAyeal, and G. A. Milne, 2008: On the factors behind large Labrador Sea tides during the last glacial cycle and the potential implications for Heinrich events. *Paleoceanography*, **23**, PA3211, doi:10.1029/2007PA001573.

Birch, F., 1964: Density and Composition of Mantle and Core. *Journal of Geophysical Research Atmospheres*, **69(20)**, 4377-4388.

Bowman, M. J., A. C. Kibblewhite, R. A. Murtagh, S. M. Chiswell, B. G. Sanderson, 1983: Circulation and mixing in greater Cook Strait, New Zealand. *Oceanol. Acta.*, **6(4)**, 383-391.

Burša, M., 1993: Parameters of the earth's tri-axial level ellipsoid. *Studia Geophysica et Geodaetica*, **37(1)**, 1-13.

Caldwell, P. C., M. A. Merrfield, P. R. Thompson, 2015): Sea level measured by tide gauges from global oceans — the Joint Archive for Sea Level holdings (NCEI Accession 0019568), Version 5.5, NOAA National Centers for Environmental Information, Dataset, doi:10.7289/V5V40S7W.

Cartwright. D. E., A. C. Edden, R. Spencer, J. M. Vassie, 1980: The tides of the northeast Atlantic Ocean. *Philosophical Transactions of the Royal Society of London*, **A298**, 87-139.

Cartwright, D. E., 1999: *Tides: A Scientific History*. Cambridge University Press.

Deacon, M., 1971: *Scientists and the Sea, 1650-1900*. Academic Press (London).

Doodson, A. T. and H. D. Warburg, 1941: *Admiralty Manual of Tides*. London HMSO.

Eanes, R., and S. Bettadpur, 1996: The CSR 3.0 global ocean tide model. *Tech. Memo.* CSR-TM-96-05, Center for Space Res., Univ. Texas, Austin.

Egbert, G. D., and S. Y. Erofeeva, 2002: Efficient inverse modeling of barotropic ocean tides. *J. Atmos. Oceanic Tech.*, **19**, 183-204.

Egbert, G. D., R. D. Ray, and B. G. Bills, 2004: Numerical modeling of the global semidiurnal tide in the present day and in the last glacial maximum. *J. Geophys. Res.*, **109**, C03003, doi:10.1029/2003JC001973.

Farrell, W. E., 1973: earth tides, ocean tides and tidal loading. *Philosophical Transactions of the Royal Society of London*, **A274**,253-259.

Fowler, C. M. R., 2004: *The Solid earth: An Introduction to Global Geophysics (2nd Education)*. Cambridge University Press.

Fu, L.-L. and A. Cazenave, 2001: *Satellite Altimetry and earth Sciences*. Academic Press, San Diego, Calif.

Gao, Z. Z., Y. B. He, X. D. Li, T. Z. Duan, 2013: Review of research in internal-wave and internal-tide deposits of China. *Journal of Palaeogeography*, **2 (1)**, 56-65.

Gargett, A. E., B. A. Hughes, 1972: On the interaction of surface and internal waves. *Journal of Fluid Mechanics*, **52**, 179-191.

Garrett, C., W. Munk, 1979: Internal waves in the ocean. *Annual Review of Fluid Mechanics*, **1**, 339-369.

Heiskanen, W. A., 1962: Is the earth a triaxial ellipsoid?. *J. geophys. Res.*, **67 (1)**, 321-327.

Hendershott, M. C., 1972: The effects of solid earth deformation on global ocean tides. *Geophysical Journal of the Royal astronomical Society*, **29**, 389-402.

Herndon, J. M., 1980: The chemical composition of the interior shells of the earth. *Proc. R. Soc. Lond.*, **A372(1748)**, 149-154.

Herndon, J. M., 2005: Scientific basis of knowledge on earth's composition. *Current Science*, **88(7)**, 1034-1037.

Hill, D. F., S. D. Griffiths, W. R. Peltier, B. P. Horton, and T. E. Tornqvist, 2011: High-resolution numerical modeling of tides in the western Atlantic, Gulf of Mexico, and Caribbean Sea during the Holocene. *J. Geophys. Res.*, **116**, C10014, doi:10.1029/2010JC006896.

Jordan, T. H., 1979: Structural Geology of the earth's Interior. *Proc. Natl. Acad. Sci. USA.*, **76 (9)**, 4192-4200.

Kaula, W. M., 1968: *Introduction to Planetary Physics: the Terrestrial Planets*. John Wiley.

Kopal, Z., 1969: *Dynamics of the earth-moon System*. Springer Netherlands.

Lambeck, K., 1988: *Geophysical Geodesy*. Clarendon Press, Oxford.

Lide, D. R., 2000: *Handbook of Chemistry and Physics (81st ed.)*.

Longman, I. M., 1963: A Green's function for determining the deformation of the earth under surface mass loads. *J. geophys. Res.*, **68**, 485-496.

Love, A. E. H., 1909: The Yielding of the earth to Disturbing Forces. *Proc. Roy. Soc. London*, **82**, 73-88.

Luzum, B., and Coauthors, 2011: The IAU 2009 system of astronomical constants: The report of the IAU working group on numerical standards for Fundamental Astronomy. *Celestial Mechanics and Dynamical Astronomy*, **110(4)**, 293-304.

Melchior, Paul., 1974: earth Tides. *Surveys in Geophysics*, **1**, 275-303.

Monnereau, M., M. Calvet, L. Margerin, A. Souriau, 2010: Lopsided Growth of earth's Inner Core. *Science*, **328(5981)**, 1014-1017.

Munk, W., 1997: Once again-Tidal friction. *Progr. Oceanogr.*, **40**, 7-35.

National Research Council (U.S.)., 1964: *Panel on Solid earth Problems. Solid-earth Geophysics: Survey and Outlook*. National Academies.

National Research Council (U.S.)., 1993: *Solid-earth sciences and society*. National Academy Press, Washington.
Ozawa, H., F. Takahashi, K. Hirose, Y. Ohishi, N. Hirao, 2011: Phase Transition of FeO and Stratification in earth's Outer Core. *Science*, 3**34(6057)**, 792-794.
Parke, M. E., and M. C. Hendershott, 1980: M_2, S_2, K_1 models of the global ocean tide on an elastic earth. *Mar. Geod.*, **3**, 379-408.
Pekeris, C. L. and Y. Accad, 1969: Solution of Laplace's equations for the M2 tide in the world oceans. *Philos. Trans. R. Soc. A.*, **A265**, 413-436.
Phillips, O. M., 1974: Nonlinear dispersive waves. *Annual Review of Fluid Mechanics*, **6**, 93-110.
Pidwirny, M., 2006: *Introduction to the Oceans (Fundamentals of Physical Geography, 2nd Edition)*.
Provost, C. L., M. L. Gence, F. Lyard, 1994: Spectroscopy of the world ocean tides from a finite element hydro dynamic model. *J. Geophys. Res.*, **99**, 24777-24797.
Pugh, D. T., 1987: *Tides, Surges and Mean Sea-Level*. JOHN WILEY & SONS.
Pugh, D. T. and P. L. Woodworth, 2014: *Sea-Level Science: Understanding Tides, Surges Tsunamis and Mean Sea-Level Changes*. Cambridge Univ. Press, Cambridge.
Ray, R. D., 1999: A global ocean tide model from Topex/Poseidon altimetry: GOT99.2. *NASA Tech. Memo.* 209478, 58 pp., Goddard Space Flight Center, Greenbelt, MD.
Robert, H. S., 2008: *Introduction To Physical Oceanography*. Texas A& M University.
Roy, A. E., 1978: *Orbital Motion*. Adam Hilger, Bristol.
Scherneck, H.-G., 1991: A parametrized solid earth tide model and ocean tide loading effects for global geodetic baseline measurements. *Geophys. J. Int.*, **106(3)**, 677-694.
Schettino, A., 2014: *Quantitative Plate Tectonics*. Springer International Publishing.
Schureman, P., 1976: *Manual of Harmonic Analysis and Prediction of Tides*. United States Government Printing Office, Washington.
Schwiderski, E. W.,1979: Global ocean tides: Part II. The semidiurnal principal lunar tide 84 (M_2), Atlas of Tidal Charts and Maps. *NSWC Tech. Rep.*, 79-414.
Segar, D. A., 2012: *Waves Introduction to Ocean Sciences (electric book), 2nd edition*.
Shum, C. K., et al., 1997: Accuracy assessment of recent ocean tide models. *J. Geophys. Res.*, **102**, 25,173-25,194.
Shanmugam, G., 2014: Review of research in internal-wave and internal-tide deposits of China: Discussion. *Journal of Palaeogeography*, **3**, 332-350.
Shepard, F. P., 1975: Progress of internal waves along submarine canyons. *Marine Geology*, **19**, 131-138.
Simon, J. L., P. Bretagnon, J. Chapront, M. Chapront-Touze, G. Francou, J. Laskar, 1994: Numerical expressions for precession formulae and mean elements for the moon and planets. *Astronomy and Astrophysics*, **282 (2)**, 663-683.
Smart, W. M., 1940: *Spherical Astronomy*. Cambridge University Press.
Stammer, D., and Coauthors, 2014: Accuracy assessment of global barotropic ocean tide models. *Rev. Geophys.*, **52**, 243-282.
Stevens, C. L., M. J. Smith, B. Grant, C. L. Stewart, T. Divett, 2012: Tidal Stream Energy Extraction in a Large Deep Strait: the Karori Rip, Cook Strait. *Continental Shelf Research*, **33**, 100-109.
Stixrude, L. and R. E. Cohen, 1995: High-Pressure Elasticity of Iron and Anisotropy of earth's Inner Core. *Science*, **267 (5206)**, 1972-1975.
Vlasenko, V., N. Stashchuk, K. Hutter, 2005: *Baroclinic Tides: Theoretical Modeling and Observational Evidence*. Cambridge Univ. Press, Cambridge.

Visser, P. N. A. M., N. Sneeuw, T. Reubelt, M. Losch, T. Van Dam, 2010: Space-borne gravimetric satellite constellation and ocean tides: Aliasing effects. *Geophys. J. Int.*, 181, 789-805.

Voigt, C., et al., 2016: Report on the Data Base of the International Geodynamics and earth Tide Service (IGETS), (Scientific Technical Report STR – Data; 16/08), Potsdam: GFZ German Research Centre for Geosciences.DOI:doi.org/10.2312/GFZ.b103-16087.

Wootton, A., 2006: earth's Inner Fort Knox. *Discover*, **27 (9)**, 18.

Wieczorek, M. A., and Coauthors, 2006: The constitution and structure of the lunar interior. *Reviews in Mineralogy and Geochemistry*, **60(1)**, 221-364.

Williams, D. R., 2013: *sun Fact Sheet, NASA Goddard Space Flight Center*.